Quasielastic electron scattering from ^{40}Ca

C. F. Williamson, T. C. Yates,* W. M. Schmitt, and M. Osborn †
Bates Linear Accelerator Center and Department of Physics, MIT, Cambridge, Massachusetts 02139

M. Deady
Department of Physics, Bard College, Annandale-on-Hudson, New York 12504

Peter D. Zimmerman‡ and C. C. Blatchley§
Department of Physics and Astronomy, Louisiana State University, Baton Rouge, Louisiana 70803

Kamal K. Seth, M. Sarmiento, and B. Parker‖
Department of Physics and Astronomy, Northwestern University, Evanston, Illinois 60208

Yanhe Jin, L. E. Wright, and D. S. Onley
Institute of Nuclear and Particle Physics, Ohio University, Athens, Ohio 45701

(Received 13 June 1997)

Differential cross sections for quasielastic electron scattering on ^{40}Ca have been measured at laboratory scattering angles of 45.5°, 90°, and 140° with bombarding energies ranging from 130 to 840 MeV. Transverse and longitudinal response functions have been extracted for momentum transfers from 300 to 500 MeV/c. Contrary to some previously reported results, the total observed longitudinal strength agrees with the relativistic Fermi gas prediction to within ±18%. [S0556-2813(97)00112-X]

PACS number(s): 25.30.Fj

I. INTRODUCTION

Medium energy electron scattering has proven to be one of the most useful tools in the study of nuclear structure. Quasielastic scattering of electrons by a nucleus provides insight into the distribution of charges and currents in the nucleus. In this paper we present results of measurements of differential cross sections for quasielastic scattering from ^{40}Ca and the deduced longitudinal and transverse response functions for momentum transfers up to 500 MeV/c. A brief report of the results of this experiment was published earlier [1].

II. THEORETICAL FORMALISM

The cross sections for quasielastic electron scattering can be described in the one-photon-exchange plane wave Born approximation by the Rosenbluth formula

$$\frac{d^2\sigma}{d\Omega\, d\omega} = \sigma_{\mathrm{Mott}} S_{\mathrm{tot}}(q,\omega,\theta), \tag{1}$$

with

$$S_{\mathrm{tot}}(q,\omega,\theta) = \left|\frac{Q^2}{q^2}\right|^2 R_L(q,\omega) + \left(\frac{|Q|^2}{2q^2} + \tan^2\frac{\theta}{2}\right) R_T(q,\omega), \tag{2}$$

where

θ = laboratory scattering angle,

Ω = solid angle,

ω = energy loss,

$R_L(q,\omega)$ = longitudinal response function,

$R_T(q,\omega)$ = transverse response function,

q = three-momentum transfer,

$Q^2 = q^2 - \omega^2$,

σ_{Mott} = Mott scattering cross section,

and

*Present address: Andersen Consulting, Columbus, OH 43215.
†Present address: General Research Corporation, Danvers, MA 01923.
‡Present address: Institute for Defense Analysis, Alexandria, VA.
§Present address: Department of Physics, Pittsburg State University, Pittsburg, KS 66762.
‖Present address: DESY, D-22607 Hamburg, Germany.

$$q^2 = 4E_i(E_i - \omega)\sin^2\frac{\theta}{2} + \omega^2,$$

$$\sigma_{\text{Mott}} = \left(\frac{\alpha\hbar c\cos(\theta/2)}{2E_i\sin^2(\theta/2)}\right)^2,$$

E_i = total incident electron energy.

It is convenient to write Eq. (2) in a form in which the independent variable ranges from 0 to 1 rather than from 0 to ∞. This can be done in terms of the virtual photon polarization $\epsilon(\theta)$ where

$$\epsilon(\theta) = \left[1 + \frac{2q^2}{Q^2}\tan^2\frac{\theta}{2}\right]^{-1}. \tag{3}$$

Then Eq. (1) becomes

$$\epsilon(\theta)\left(\frac{1}{\sigma_{\text{Mott}}}\right)\left(\frac{q^4}{Q^4}\right)\frac{d^2\sigma}{d\Omega d\omega} = \epsilon(\theta)R_L(q,\omega) + \frac{1}{2}\left(\frac{q^2}{Q^2}\right)R_T(q,\omega). \tag{4}$$

By defining

$$S_{\text{tot}}(q,\omega,\epsilon) = \left(\frac{\epsilon(\theta)}{\sigma_{\text{Mott}}}\right)\left(\frac{q^4}{Q^4}\right)\frac{d^2\sigma}{d\Omega d\omega},$$

Eq. (4) becomes

$$S_{\text{tot}}(q,\omega,\epsilon) = \epsilon(\theta)R_L(q,\omega) + \frac{1}{2}\left(\frac{q^2}{Q^2}\right)R_T(q,\omega). \tag{5}$$

Equation (5) describes a straight line in the independent variable $\epsilon(\theta)$ with slope $R_L(q,\omega)$ and intercept proportional to $R_T(q,\omega)$. It is clear from Eqs. (2) and (5) that R_L and R_T can in principle be extracted from differential cross sections measured at two or more scattering angles but at incident energies such that they have the same three-momentum transfer.

The quasielastic response functions in Eq. (2) reflect the structure and momentum distribution of the ensemble of the nucleons in the nucleus. Roughly speaking, in quasielastic electron scattering R_L carries information about the static charge distribution of the nucleons, and R_T carries information about the current and magnetization distributions of the nucleons.

The electron is a very light particle and therefore tends to radiate readily, especially during the scattering process. The experimental data must be corrected for these radiative processes in order to obtain the true nuclear response to the scattering. The incoming electron waves are also significantly distorted by the nuclear Coulomb field, and these distortion effects must be corrected if one wishes to compare experimental results with the above plane-wave Born approximation (PWBA) formalism. The mathematical formalism has been developed for making these corrections, and its application to the present data to extract the response functions will be discussed in subsequent sections.

III. BRIEF REVIEW OF PREVIOUS WORK

The usefulness of incoherent scattering of high-energy electrons from nucleons in nuclei for studying the structure and momentum distribution of nucleons bound in nuclei has been long recognized. One of the first such experiments was carried out at Stanford [2]. This experiment on Be and C clearly showed both the peak due to quasielastic scattering and the peak due to Δ-isobar excitation. In the following 14 years a number of quasielastic electron scattering experiments were reported from laboratories at Orsay [3–9], Harvard [10,11], Khark'ov [12–16], and DESY [17]. These experiments were for the most part somewhat fragmentary in that they were often performed at one or two bombarding energies and at a single scattering angle. There was no systematic study of the mass dependence of the properties of quasielastic scattering, and there was no data set that would allow extraction of separated longitudinal and transverse response functions. However, these early experiments did provide a database for testing the theories of quasielastic scattering that existed at that time [18–30].

The first systematic study of quasielastic scattering properties as a function of mass number was carried out at the Mark III linac at Stanford [31,32]. These data were taken at a constant energy of 500 MeV and constant angle of 60° and included nine nuclei from mass 6 to mass 208. Since data were taken only at one bombarding energy and scattering angle, separation into longitudinal and transverse response functions was not possible. The semirelativistic Fermi gas theory of Moniz [26] was used to extract the Fermi momentum and effective binding energy by fitting to the quasielastic spectrum. The fitted values of these parameters varied fairly smoothly with mass number and agreed reasonably well with estimates based on the nuclear sizes. The theoretical curves with the fitted Fermi momentum and effective binding energy gave a remarkably good account of the data in the quasielastic region of the spectrum, although at larger energy losses the theory fell well below the data even when meson exchange currents, meson production, and Δ-isobar excitation were included in the theory. This was especially marked in the energy loss region between the quasielastic peak and the Δ resonance. An early attempt was also made to extract separated longitudinal and transverse response functions from these and subsequent data taken at Mark III [33,34].

The fact that the data of Whitney *et al.* [32] could be fit quite well with a very simple nuclear model seemed to indicate that the quasielastic process might be reasonably well understood, although it was clear that the theory for meson and isobar effects was deficient. At about this time new facilities were beginning operation at MIT and Saclay that could produce very high-quality electron beams at energies of several hundred MeV, and that were equipped with a new generation of precision magnetic spectrometers. These new facilities permitted data to be acquired over a wide kinematic range at several scattering angles to allow separation of the transverse and longitudinal responses. Theoretical efforts also continued to refine the models for quasielastic scattering [35–43].

The first experiment specifically designed to yield separated transverse and longitudinal response functions was reported by Altemus *et al.* [44]. In this Bates experiment quasi-

elastic electron scattering from ^{56}Fe was observed over a momentum transfer range of $210 \leqslant q \leqslant 410$ MeV/c. The transverse response functions seemed to agree reasonably well with the predictions of the Fermi gas model. However, the total longitudinal strength showed a startling tendency with increasing momentum transfer. At $q = 210$ MeV/c the experiment and theory agreed reasonably well, but with increasing q the measured longitudinal strength decreased steadily with respect to the theory until it was only about 50% of the theoretical value at $q = 410$ MeV/c. Since the total longitudinal strength should be only slightly model dependent and at high momentum transfers should be very simply related to the total charge in the nucleus, it was very difficult to explain these results in the framework of conventional models of nuclear structure.

Separated response functions were also extracted for quasielastic electron scattering from ^{40}Ca and ^{48}Ca [45,46] at Bates for momentum transfers up to of 410 MeV/c. These experiments were consistent with some longitudinal suppression. However, a careful analysis of the systematic errors yielded an uncertainty of at least $\pm$ 20% in the total longitudinal strength, resulting in a somewhat ambiguous conclusion.

Separated quasielastic response functions were also reported by the Saclay group on ^{12}C [47] over a momentum transfer range of $200 \leqslant q \leqslant 500$ MeV/c. In the case of this rather light nucleus the separated response functions agreed reasonably well with those predicted by the Fermi gas model. Subsequent work at Saclay on the nuclei ^{40}Ca, ^{48}Ca, and ^{56}Fe [48,49] seemed to verify the results of Altemus *et al.*, in that the total longitudinal strength at a momentum transfer of 550 MeV/c seemed to be 30–40 % below the Fermi gas predictions.

The above experimental results showing a strong reduction in the total longitudinal strength compared to the relativistic Fermi gas model have inspired a large number of theoretical papers attempting to account for the effect [50–62]. Many of these theoretical calculations were able to achieve a reduction in the longitudinal responses sufficient to correspond approximately with the Saclay results, but this invariably resulted in an unacceptably bad fit to the transverse responses [63].

The situation was further complicated by recent experimental results from Bates and Saclay. The Bates results for quasielastic scattering on ^{238}U [64] at a momentum transfer of 500 MeV/c indicated that the total longitudinal strength was 95 $\pm$ 15 % of that predicted by the Fermi gas model. On the other hand, the Saclay results for quasielastic scattering on ^{208}Pb [65] showed a reduction in the total longitudinal strength of greater than 50% relative to the Fermi gas model at a momentum transfer of 550 MeV/c. A comparison of the Bates ^{238}U and Saclay ^{208}Pb results for the integrated longitudinal strength as a function of three-momentum transfer is shown in Fig. 1.

New results from Bates for quasielastic scattering from ^{40}Ca [1] showed about 85% of the total expected longitudinal strength at a momentum transfer of 450 MeV/c with an overall uncertainty of about $\pm$ 15%. These results were in strong disagreement with the Saclay results of Ref. [49]. A comparison of the Bates and Saclay results for the integrated longitudinal strength for inclusive quasielastic scattering from ^{40}Ca is shown in Fig. 2. The present paper is a more complete presentation of the results given in Ref. [1].

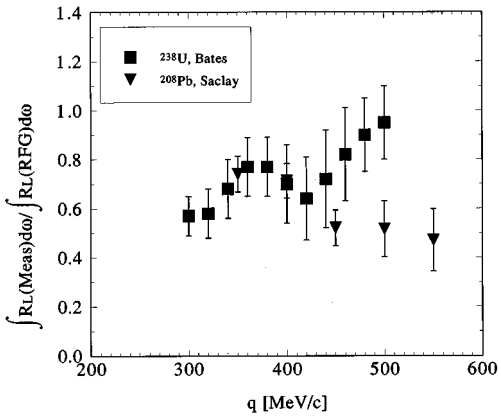

FIG. 1. Comparison of the measured total longitudinal strengths for quasielastic scattering from ^{208}Pb (Saclay, inverted triangles) [65] and ^{238}U (Bates, squares) [64] as a function of three-momentum transfer. The longitudinal strengths have been normalized by dividing the experimental results by the total strength predicted by the relativistic Fermi gas model.

IV. EXPERIMENTAL ARRANGEMENT

The measurements described in this paper were carried out at the MIT Bates Linear Accelerator Center. Electron beams in the energy range 130 to 840 MeV were produced by the Bates electron linac [66]. Beam currents up to 35 μA were used. The charge passing through the target for each run was measured by a nonintercepting toroid and integrated to an accuracy of approximately 0.1%.

The ^{40}Ca target used in this experiment was a self-supporting foil of natural calcium ($\approx$97% ^{40}Ca) having an average thickness of approximately 100 mg/cm^2. The target was stored, measured, and transferred under inert atmosphere or vacuum to prevent chemical deterioration. The average thickness was measured before and after each transfer from the target laboratory to the scattering chamber by weighing the foil with a precision balance and carefully measuring its physical area. It was observed that over the time period of

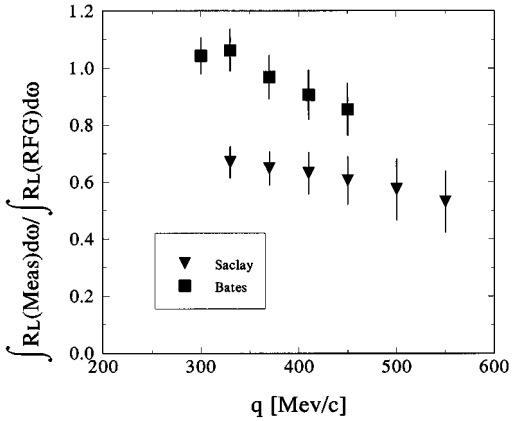

FIG. 2. Comparison of the measured total longitudinal strengths for quasielastic scattering from ^{40}Ca as reported from Saclay (inverted triangles) [49] and Bates (squares) [1].

this experiment the thickness of this target did not change by more than 3%.

Besides ^{40}Ca, several other targets (BeO, C, etc.) were used for calibration purposes. These were installed in a standard target ladder. The target ladder, containing up to eight targets, was contained in a vacuum enclosure which could be coupled to the scattering chamber, and this ladder could be transferred into the scattering chamber without breaking the vacuum. The design of the scattering chamber allowed an uninterrupted vacuum from the target to the exit vacuum window in the spectrometer just before the detector systems. Changing the scattering angle of the spectrometer required bringing the scattering chamber and a short section of the spectrometer vacuum to atmospheric pressure. This could be accomplished without exposing the targets to air. The design of the scattering chamber allowed continuous angular coverage from 45.50° to 140.00°. The design of the spectrometer also allowed continuous coverage of this angular range, and the scattering angle could be set with an accuracy of $\pm 0.01°$.

The scattered electrons were momentum analyzed by the vertical bend Bates energy loss spectrometer system (ELSSY) [67]. The acceptance solid angle of ELSSY was determined by two sets of independently variable slits for the horizontal and vertical directions placed approximately 1.8 m from the target. Typical openings were 5 cm horizontal by 25 cm vertical, and the reproducibility of these settings was better than $\pm$ 0.03 cm. The maximum solid angle acceptance used in this experiment was about 3.4 msr.

The spectrometer system is dispersion matched, with the beam on the target dispersed to match the dispersion of ELSSY. The typical energy spread of the beam from the linac was $\pm$ 0.15%, and the dispersion resulted in a beam spot size on the target of about 0.3 cm (h) $\times$ 2.5 cm (v). This had the advantage of sampling a fairly large area of target so that the effective target thickness was insensitive to local variations in thickness and therefore was accurately represented by the measured average thickness. The resulting momentum resolution of ELSSY was typically $\Delta p/p \approx 10^{-4}$.

The momentum analyzed electrons were recorded by a detector system located just beyond the exit vacuum window of ELSSY. A schematic diagram of this system is shown in Fig. 3. The first element in this system was a vertical drift chamber (VDC) [68] tilted at an angle of 45° with respect to the optical axis of ELSSY and lying approximately at the focal surface. This VDC measured the incident electron angle in the dispersion plane with respect to the central optical axis of ELSSY to an accuracy of about $\pm$ 15 mr. It also measured the position of the intersection of the electron trajectory with the axis of the VDC to an accuracy of about ± 0.1 mm. From these two quantities it was possible to determine the intersection of the electron trajectory with the actual focal surface and thus determine the electron momentum with an uncertainty of $\Delta p/p \approx 10^{-4}$.

The second element in the detector system was a drift chamber whose wires were parallel to the direction of dispersion. This drift chamber, referred to as the transverse array, measured the distance of intersection of the electron trajectory in the direction perpendicular to the dispersion direction. This made possible a correction for angular kinematic broadening across the solid angle acceptance of ELSSY.

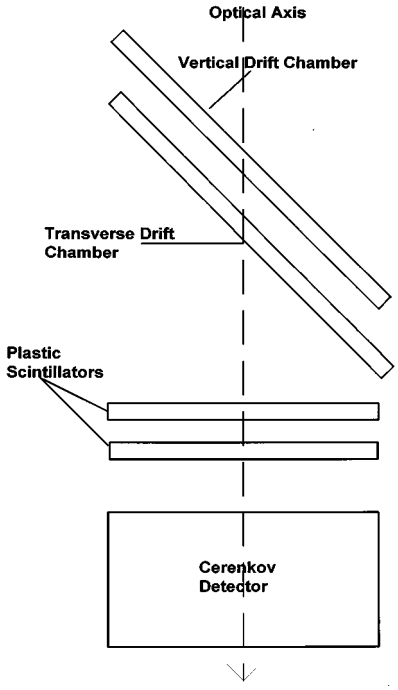

FIG. 3. Schematic diagram of the Bates ELSSY spectrometer detector system.

The third element in the detector system was a thin plastic scintillator that provided the timing triggers for all events. In the early stages of the experiment this was a single scintillator, but this was later replaced by two scintillators in coincidence to reduce background and noise triggers.

The fourth element in the detector system was a Čerenkov counter to distinguish electrons from heavier charged particles. In the earliest phase of this experiment this consisted of two 5 cm thick slabs of lucite viewed with photomultipliers and operated in coincidence to reduce accidental background and tube noise. These gave good rejection of protons and heavier charged particles, but they were not effective in eliminating charged pions and muons. These detectors were later replaced by aerogel Čerenkov detectors that were very effective in rejecting pions and muons at bombarding energies up to 700 MeV. For the final phase of the experiment at 45.5° where the bombarding energies reached 840 MeV, the aerogel detector was replaced by a gas Čerenkov detector filled with freon. This detector had a pion and muon threshold of about 2 GeV, and effectively eliminated all heavy charged particle contamination.

The signals from the various detectors were fed to a CAMAC based data acquisition system. The CAMAC units were interfaced to the data acquisition computer by a microprogrammed branch driver. In the earlier phases of this experiment the data acquisition computer was a PDP-11 which acquired data in on-line mode. This was replaced in the latter phases of the experiment by a Microvax II computer operating in event mode data acquisition that allowed off-line data replay and analysis.

V. DATA ACQUISITION

The useful momentum range of ELSSY using the detector systems described in Sec. IV was about $\pm$ 2.5%. The inelas-

tic momentum range of interest in this experiment varied from about 50 to about 85 % of the total, depending upon the bombarding energy. Therefore, it was necessary to acquire the data by taking a number of runs for different values of spectrometer magnetic field in order to cover the desired range of momenta. Due to limitations in running time it was not practical to take enough data runs to provide continuous coverage of the entire momentum range. However, the energy separation between successive magnet settings was always kept small compared to the width of the quasielastic peak.

In addition to the quasielastic scattering it was possible over part of the kinematic range to have a contribution to the electron spectrum from secondary e^+e^- pair production. Since pair production is a charge symmetric process, this contribution to the inelastic cross sections was determined by reversing the spectrometer polarity and measuring the corresponding positron spectrum. In general, the pair production contributed at most only a few percent to the inelastic spectrum.

Since data were acquired at very deep inelasticity, corresponding to quite small outgoing electron energy, there was some concern that at the higher energies there might be a measurable contribution from electrons that penetrated the spectrometer acceptance defining slits. These were made of tungsten alloy and were 5 cm in thickness, corresponding to about 15 radiation lengths. Calculations made using the formalism of Rossi and Greissen [69] of the total transmission of electrons through 15 radiation lengths of tungsten indicated that no more than 2% of the incident electrons would penetrate the slits at the highest bombarding energy of this experiment. The spectrum of the penetrating electrons would be very broad, with the strength strongly shifted to very low energies, so that an even smaller fraction would actually be transmitted through the magnetic spectrometer in such a manner as to contribute to the measured inelastic spectrum.

There was also a potential concern for the contribution of electrons scattered from the interior structure of ELSSY. This was a particular worry in the dispersion plane since at large inelasticities the electrons in the parts of the spectrum well above and below the central momentum could strike the vacuum enclosure of the spectrometer and produce a featureless inelastic spectrum which could not be distinguished from the almost featureless quasielastic spectrum. In the design of ELSSY these vacuum enclosures were fitted with lead baffles that were designed to intercept all possible first scatterings from the vacuum enclosure walls. In the direction transverse to the dispersion the concern was for scattering from the pole structures. However, the optics of ELSSY are such that displacement in this direction is directly related to the scattering angle. Therefore, it was possible to avoid striking the pole structures by restricting the horizontal opening of the solid angle defining slits.

In addition to these mechanical safeguards, the data analysis code allowed placing a software restriction on the angle of incidence of an electron trajectory. This greatly restricted the possible phase space accessible to an electron scattered internally in ELSSY. The angle spectra in both planes were recorded, and no indication of internal scattering was ever observed.

It was discovered, however, from spectra taken with very small horizontal slit opening that there was an extraneous source of scattering from the edges of the exit aperture of the scattering chamber. This problem affected some of the early runs in this experiment. Several runs at different energies were taken to investigate this effect, and a fairly simple analytic model of the process was developed that reproduced the effect to within a few percent. Thus, a reliable correction of no more than 15 ± 1.5 % was applied to the data already acquired. The problem was eliminated for subsequent runs by increasing the width of this aperture enough so that the electrons scattered from its edges fell outside the acceptance phase space of ELSSY.

The lucite Čerenkov detector used in the early phases of this experiment presented some problems. It was clear from the spectra taken at reversed spectrometer polarity that there was a significant contribution from pions at the larger inelasticities in the higher energy runs. In 1981 the lucite Čerenkov detector was replaced with an Aerogel detector which allowed the elimination of pion contributions in subsequent runs. Data taken with the Aerogel system were used to perform a subtraction of the pion contribution in the older data. A summary of the data runs and the type of Čerenkov detector used in each is given in Table I.

The systematic errors assigned to the data, $\pm$ 4% for the 140° runs and $\pm$ 6% for the 90° runs, reflect the confidence in the various corrections that were applied. The data at 45.5° were taken with a gas Čerenkov detector using event mode recording that allowed off-line replay. The 45.5° data were assigned a systematic error of $\pm$ 3%.

VI. DATA REDUCTION

A. Corrections for detector efficiency

The first correction applied to the data was for the efficiency of the focal plane detector system. This was determined by observing the elastic scattering peak from ^{12}C in the ELSSY focal plane detector system. The spectrometer magnetic field was varied so that the elastic peak was moved from one end of the detector system to the other in 10–12 steps. The elastic peak from each setting was fit to a modified Gaussian function with radiative tail. The total elastic scattering events were calculated by applying the proper radiative corrections. This allowed determining the relative efficiency of the focal plane detectors as a function of position in the focal plane. The statistical accuracy of the measurement was about $\pm$ 1%. The absolute efficiency was limited to $\pm$ 3% by the accuracy with which the ^{12}C differential cross sections were known. This measurement was made for each of the Čerenkov detectors used in the experiment.

The efficiency corrected data were summed into momentum bins of relative width 1–5 %. These were then converted to differential cross sections using the target thickness, integrated charge, and solid angle acceptance recorded for each run. Appropriate corrections were made for detector dead time (usually $<$10%). Since the ELSSY momentum acceptance was only about 5%, a number of such data sets were required to construct the inelastic spectrum.

B. Radiative and ionization loss corrections

These inelastic spectra still contained contributions due to the radiative tail of the elastic peak, the radiative tails of the

TABLE I. Experimental conditions and dates for the various runs.

Lab. scattering angle [deg]	Lab. bombarding energy [MeV]	Calendar date	Čerenkov detector
45.5	348.0	Apr., 1986	Freon gas
45.5	407.8	Jun., 1988	Freon gas
45.5	470.8	Jun., 1988	Freon gas
45.5	545.3	Apr., 1989	Freon gas
45.5	627.7	Apr., 1989	Freon gas
45.5	680.8	Apr., 1986	Freon gas
45.5	739.3	Apr., 1986	Freon gas
45.5	781.7	Apr., 1986	Freon gas
45.5	840.7	Jun., 1988	Freon gas
90.0	150.2	Jun., 1979	Plastic
90.0	199.8	Nov., 1979	Plastic
90.0	248.3	Jun., 1979	Plastic
90.0	297.8	Jun., 1979	Plastic
90.0	347.4	Jun., 1979	Plastic
90.0	347.4	Nov., 1979	Plastic
90.0	347.4	Apr., 1982	Aerogel
90.0	371.6	Apr., 1979	Plastic
90.0	371.6	Nov., 1979	Plastic
90.0	371.6	Nov., 1981	Aerogel
140.0	130.1	Apr., 1979	Plastic
140.0	160.0	Apr., 1981	Aerogel
140.0	189.2	Feb., 1980	Plastic
140.0	219.0	Jun., 1979	Plastic
140.0	248.9	Apr. 1979	Plastic
140.0	248.9	Apr. 1981	Aerogel
140.0	287.9	Feb., 1980	Plastic
140.0	287.9	Apr., 1982	Aerogel
140.0	327.3	Jun., 1979	Plastic
140.0	327.3	Apr., 1981	Aerogel
140.0	366.7	Jun., 1979	Plastic
140.0	366.7	Apr., 1981	Aerogel

inelastic spectrum, and the ionization straggling tail. The correction for the elastic radiative tail could only be made by calculating the cross sections for the theoretical radiative tail and subtracting these from the measured inelastic cross sections. The elastic radiative tail contained contributions from radiation from the Coulomb field of a nucleus other than the one that caused the scattering (external radiation) and from radiation that occurred during the scattering process (internal radiation). The elastic scattering cross sections for these corrections were calculated by phase shift analysis using static charge distributions derived from existing elastic scattering measurements. The ionization straggling correction was calculated according to the formalism of Landau [70].

The present data were analyzed using the general formalism for radiative corrections of Mo and Tsai [71] and Tsai [72] for an extended nucleus using the piecewise analytical integration technique developed by Maximon and Williamson [73]. Mo and Tsai estimate that in the region of the quasielastic peak these calculations should be accurate to about $\pm$ 3%. Since in general the elastic tail contribution is only a small fraction of the total cross section in the region of the quasielastic peak, these uncertainties make a negligibly small contribution to the overall uncertainty.

At energy losses well above the quasielastic peak the strength of the elastic tail becomes an appreciable fraction of the total strength, and at scattered electron energies less than about 100 MeV the elastic radiative tail becomes the dominant contributor to the inelastic spectrum. This rise in strength is due to the contribution of scattering of low-energy electrons that have lost most of their energy due to internal bremsstrahlung. Because of the uncertainties in the theoretical calculations at large energy losses, no data were analyzed for which the contribution of the calculated elastic radiative tail was more than 25% of the total strength.

The inelastic spectrum resulting after subtracting the elastic radiative tail is still distorted by radiation and ionization straggling of the inelastically scattered electrons. A given inelastic energy interval contains additional contributions from electrons which were initially at higher energy but which lose enough energy to arrive within the given energy interval. On the other hand, electrons whose energy originally fall within the given energy interval could lose enough energy so that they are no longer observed in that interval. As in the case of the elastic radiative tail there are contributions due to internal radiation, external radiation, and ionization straggling.

The formalism for the internal bremsstrahlung process is such that one can group the contributing terms into those associated with radiation before scattering and those associated with radiation after scattering. The correction for events in which the radiation occurs after scattering is relatively straightforward since all scatterings occur at the incident electron energy. However, the correction for events in which the scattering occurs after emitting a photon is more difficult since it requires knowledge of the inelastic cross sections at all energies less than the bombarding energy. Unlike the case of elastic scattering these inelastic cross sections cannot, in general, be calculated with good confidence. Instead iterative unfolding procedures developed in Refs. [71] and [72] were used to correct the inelastic spectrum.

C. Coulomb corrections

The radiatively corrected cross sections described in the previous section still contain effects due to distortions caused by the Coulomb field of the scattering nucleus. These must be corrected in order to compare to theoretical calculations since the latter normally do not include these effects. In principle one ought to make a full distorted-wave Born approximation (DWBA) calculation of the electron wave functions in the Coulomb field of the nucleus. In practice, for medium weight nuclei it turns out that one can reproduce the corrections to an accuracy of a few percent with simple assumptions [74].

From elastic electron scattering the rms nuclear radius $r_{\rm rms}$ in [fm] can be represented quite accurately for medium and heavy nuclei by

$$r_{\rm rms}=1.02A^{1/3}=\sqrt{3/5}R,$$

where R is the equivalent mean uniform spherical radius. Then the Coulomb potential for an electron at the center of a

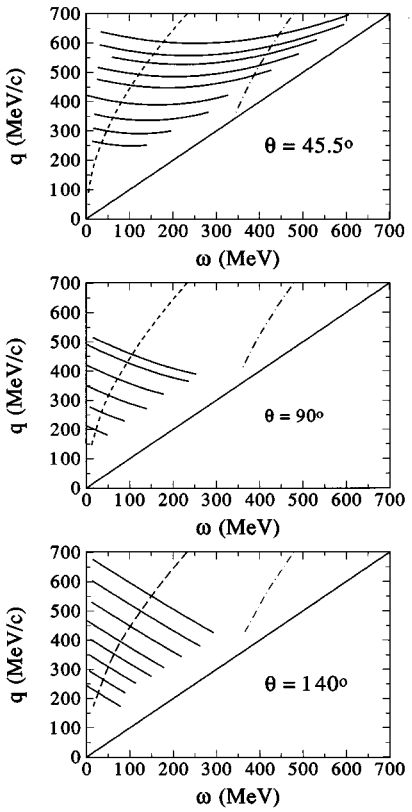

FIG. 4. Data coverage in the (q,ω) plane for this experiment. The solid curves represent the kinematics of each bombarding energy and scattering angle. The dashed curves are the approximate trajectories of the quasielastic peak, and the dot-dashed curves are the approximate trajectories of the peak of the Δ resonance.

nucleus of atomic number Z (assuming a spherical charge distribution and taking the system of units so that $\hbar=c=1$) is

$$V_c=-\frac{3\alpha Z}{2R}=-\frac{3}{2}\sqrt{\frac{3}{5}}\frac{\alpha Z}{r_{\rm rms}}. \tag{6}$$

Then an electron, whose incident momentum at infinity is p_i, making a central collision with the nucleus will have an effective momentum $p_i^{\rm eff}$ at the center of the nucleus,

$$p_i^{\rm eff}=p_i-V_c\,. \tag{7}$$

By the same argument, an electron that scatters at the center of the nucleus and has momentum p_f at infinity actually had an effective momentum $p_f^{\rm eff}$ of

$$p_f^{\rm eff}=p_f-V_c \tag{8}$$

at the point of scattering. Clearly the energy loss ω is just

$$\omega=p_i^{\rm eff}-p_f^{\rm eff}=p_i-p_f\,.$$

The effective momentum transfer $q^{\rm eff}$ is

$$q^{\rm eff}=\left[4p_i^{\rm eff}p_f^{\rm eff}\sin^2\frac{\theta}{2}+\omega^2\right]^{1/2}. \tag{9}$$

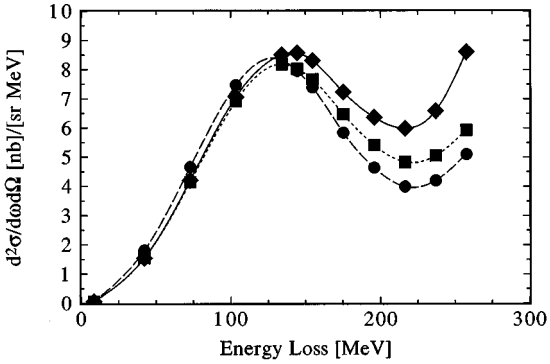

FIG. 5. Typical inelastic spectrum showing the analysis at various stages. The data corrected only for detector efficiencies are shown by diamonds. The squares show the spectrum after correction for slit scattering, pion contributions, pair-produced electrons, and the elastic radiative tail. The circles show the spectrum after radiative unfolding. The curves are drawn through the points to guide the eye.

This assumes that the incident trajectories are straight lines. In actuality the electron paths will be curved in the nuclear Coulomb field, producing a focussing effect. The lowest order correction is just an apparent increase in the incident electron flux. Conservation of angular momentum then results in an effective flux increase factor equal to $(p_i^{\rm eff}/p_i)^2$. One can therefore express the effective PWBA cross sections for the scattering in terms of the observed cross sections as

$$\left[\frac{d^2\sigma(q^{\rm eff},\theta,\omega)}{d\Omega\,d\omega}\right]_{\rm PWBA}=\left(\frac{p_i^{\rm eff}}{p_i}\right)^2\left[\frac{d^2\sigma(q^{\rm eff},\theta,\omega)}{d\Omega\,d\omega}\right]_{\rm obs}. \tag{10}$$

For ^{40}Ca, from Eq. (6) $V_c\simeq-9.6$ MeV. The smallest incident momentum was about 160 MeV/c, so the focussing effect of the Coulomb field represents a maximum correction of about 6% in p_i. Since cross sections were measured for p_f as low as 100 MeV/c, the correction in p_f could be as large as about 10%. Higher order correction terms are expected to be significantly smaller. Comparison of PWBA and DWBA calculations for quasielastic scattering in medium weight nuclei indicate that the corrections are indeed quite reliable [74].

D. Rosenbluth separations

The first step in making the Rosenbluth separations was to transform the experimental cross sections to effective PWBA cross sections according to the transformation in Eq. (10). The total response functions at constant energy E_i and laboratory scattering angle θ were calculated from

$$S_{\rm tot}(q^{\rm eff},\theta,\omega)=\frac{1}{\sigma_{\rm Mott}(E_i,\theta)}\left[\frac{d^2\sigma(q^{\rm eff},\theta,\omega)}{d\Omega\,d\omega}\right]_{\rm PWBA}. \tag{11}$$

This calculation yielded total response functions along kinematic trajectories corresponding to the incident electron momentum and laboratory scattering angle. The trajectories of the experimental spectra in the (q,ω) plane taken in this experiment are shown in Fig. 4. It is clear from this figure that

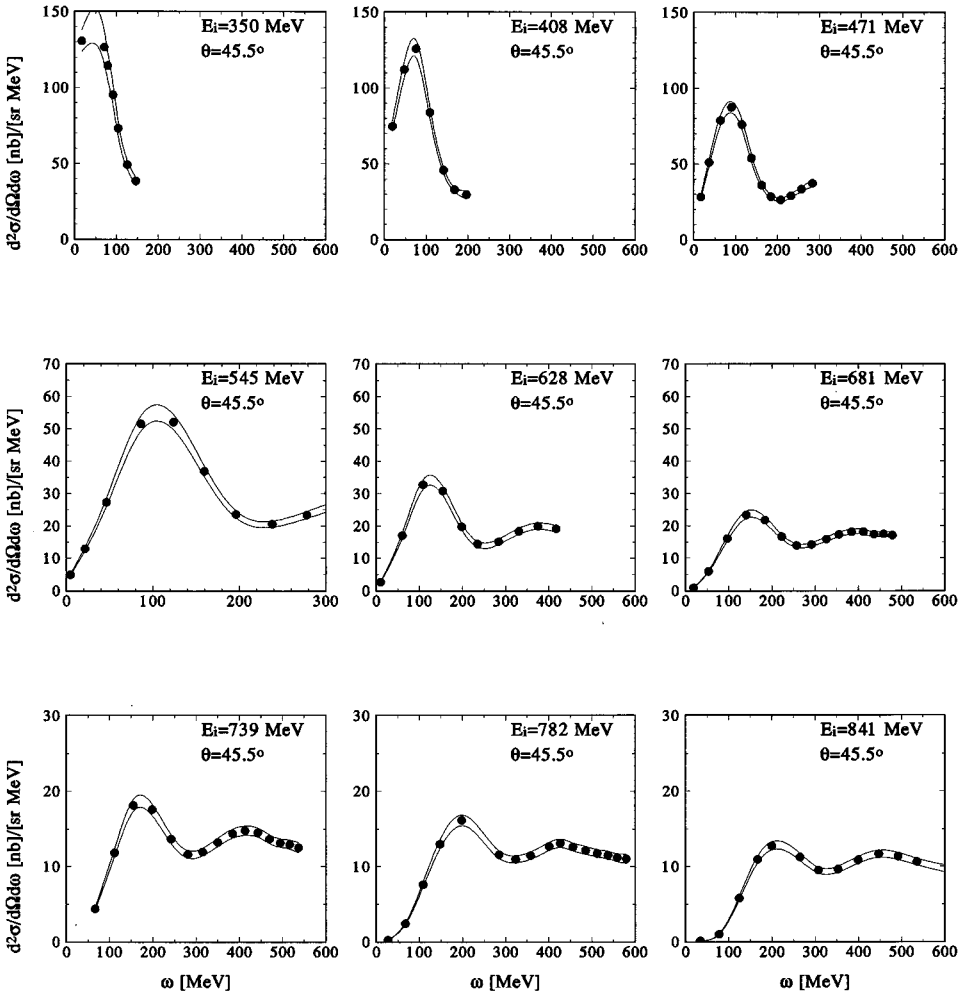

FIG. 6. Inelastic spectra observed at various bombarding energies at a laboratory scattering angle of 45.5° from ^{40}Ca. These data have been corrected for the elastic radiative tail, detector efficiencies, and pair production, and they have been radiatively unfolded. The solid curves indicate the estimated systematic error band. Statistical errors on the individual points are smaller than the symbols.

it was necessary to interpolate the data in order to construct the response functions at constant q for a given θ. For convenience in making the Rosenbluth separations the data were binned in 10 MeV intervals of ω, and a common set of values of q was used for all angles.

It was necessary to interpolate the experimental response functions in order to obtain the constant-q response functions $S_{\rm tot}(q,\omega,\theta)$. There are in principle an infinite number of trajectories in this plane along which one may interpolate to obtain $S_{\rm tot}(q,\omega,\theta)$ at the chosen grid points. It was desirable from the point of view of numerical accuracy that the interpolation trajectory be such as to minimize the changes in response function between spectra. Mo and Tsai [71] suggested interpolation along lines of constant missing mass since this would tend to line up the quasielastic peaks. An improved method was used in the present analysis using the ψ-scaling variable of Alberico *et al.* [75]. Making the transformation

$$S(q^{\rm eff},\omega,\theta)\rightarrow S(\psi,\theta), \tag{12}$$

where ψ is a function of $q^{\rm eff}$, ω, and Fermi momentum k_f, as described in Sec. VII C results in a set of response functions whose peaks are very well aligned and whose strengths vary slowly with ψ. One then interpolates this set of response functions along the value of ψ corresponding to each given (q,ω) pair on the predetermined grid to obtain $S(\psi,\theta)$ at each of these points. One then obtains $S_{\rm tot}(q,\omega,\theta)$ at each point by inverting the transformation of Eq. (12). In the present analysis interpolation polynomials of maximum order three were used to obtain $S(\psi,\theta)$.

The experimental unknowns in Eqs. (2) and (5) are the longitudinal response function $R_L(q,\omega)$ and the transverse response function $R_T(q,\omega)$. When values of $S_{\rm tot}(q,\omega,\theta)$ were available for only two values of θ the transverse and longitudinal response functions (obtained from the intercept and slope of the Rosenbluth plot) were uniquely determined. When values of $S_{\rm tot}(q,\omega,\theta)$ were available for more than two angles, the Rosenbluth plot was determined by linear regression.

E. Error analysis

In this analysis two types of errors were recognized—statistical errors and instrumental errors. Each type of error was propagated separately through the analysis. The statisti-

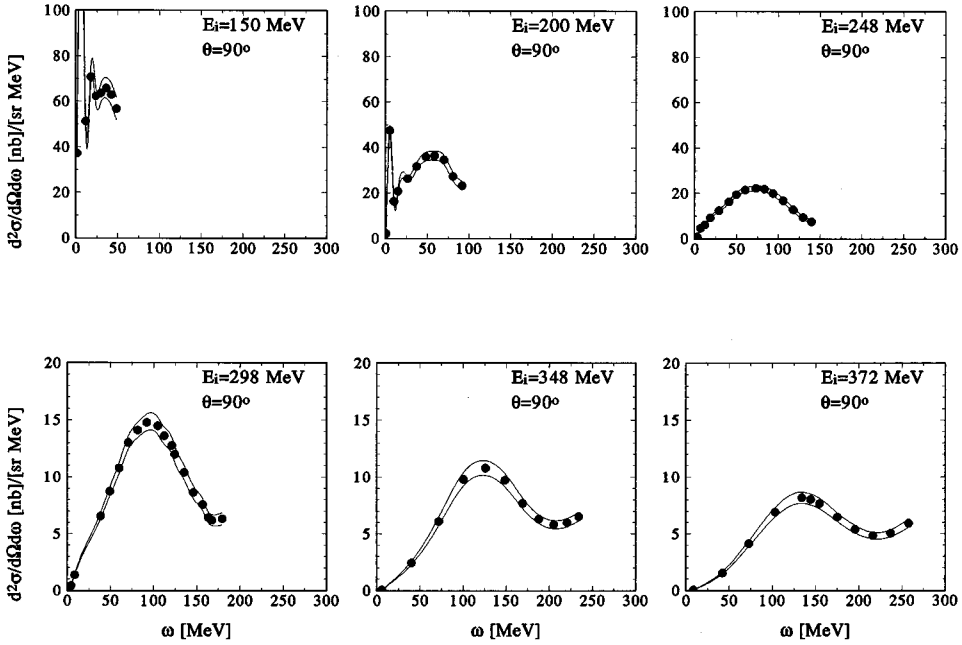

FIG. 7. Same as Fig. 6 for a laboratory scattering angle of 90°.

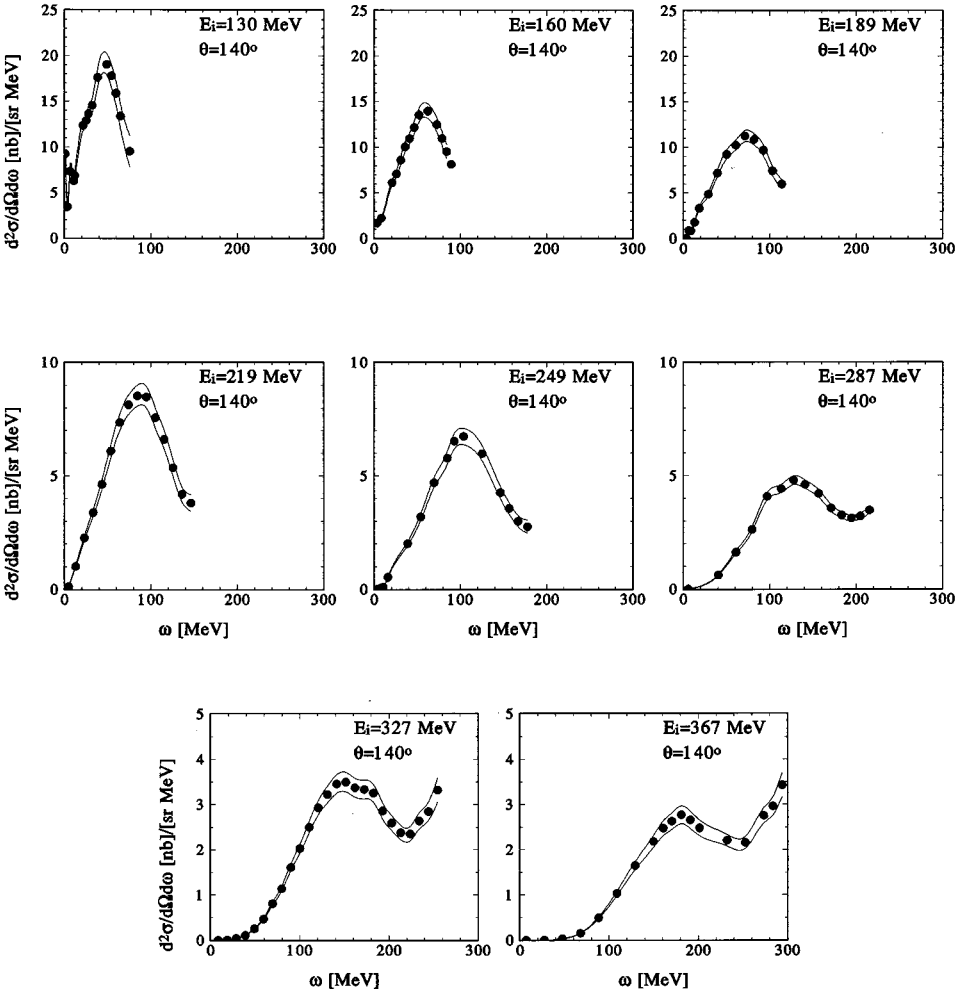

FIG. 8. Same as Fig. 6 for a laboratory scattering angle of 140°.

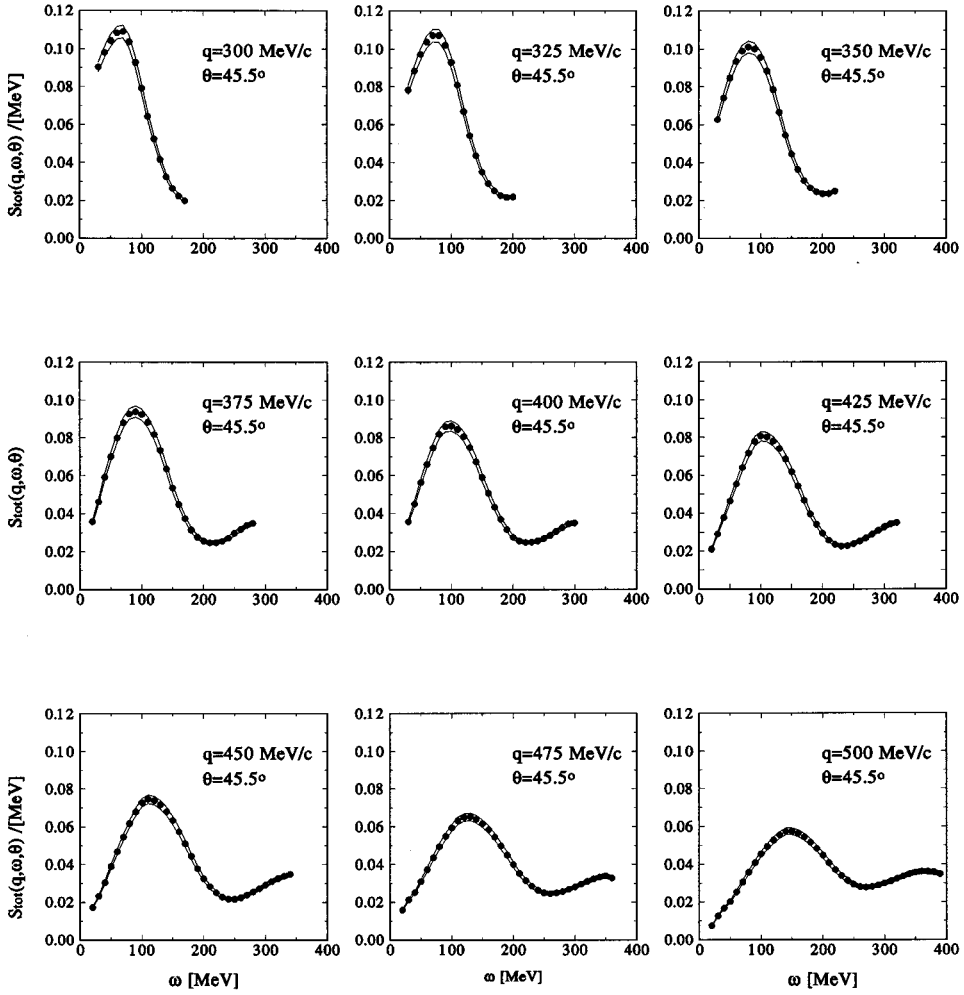

FIG. 9. Total inelastic response functions vs energy loss at constant three-momentum transfer for ^{40}Ca at a laboratory scattering angle of 45.5°. The solid curves indicate the systematic error band. Statistical errors on the individual points are smaller than the symbols.

cal errors arise from the finite number of events recorded in each momentum interval of the spectrum. These statistical errors are assumed to follow a Poisson parent distribution. However, since there were typically more than 100 events in a given momentum interval, the Poisson distribution differed negligibly from a normal distribution. Thus, all statistical errors were evaluated assuming a normal distribution. These statistical errors were propagated through all calculations in the standard way. In an interpolation calculation the variance of the resultant value was calculated as the weighted sum of the variances of each element contributing to the resultant value.

The values of systematic errors as given in Sec. V reflect the best estimates of the instrumental reproducibility of the measurement. The response functions at constant q and ω must be obtained by interpolation of different measurements, and it is not always clear how instrumental errors from different measurements should be combined. In the present analysis the systematic error in an interpolation was evaluated by interpolating the extremes of the systematic error bars. We emphasize that in general we have chosen to be extremely conservative in our estimates of systematic errors.

In all the response functions the systematic errors were significantly larger than the statistical errors. Therefore, only the systematic errors were used in the extraction of the longitudinal and transverse response functions by the Rosenbluth procedure. In the linear regression the systematic errors were taken as variances in a normal distribution. The longitudinal and transverse response functions are the fitted parameters of the regression process, and their variances are calculated in the usual way.

The total strengths of the longitudinal transitions at each value of q were obtained by integrating the longitudinal response functions over energy loss. In doing this it is very important to distinguish between the statistical and instrumental errors. Integrating over the inelastic spectrum reduces the relative statistical errors. However, the instrumental errors are expected to apply equally to all data runs. Therefore, integrating over the inelastic spectrum does not reduce the instrumental errors. The instrumental error for each integrated response was taken as one-half the difference between the area of the curve determined by the upper limits of the instrumental errors and the area under the curve determined by the lower limits of the instrumental errors.

F. Integrated response strengths

In order to compare the experimental results with theoretical calculations of integrated response strengths it is in principle necessary to have separated response functions over the

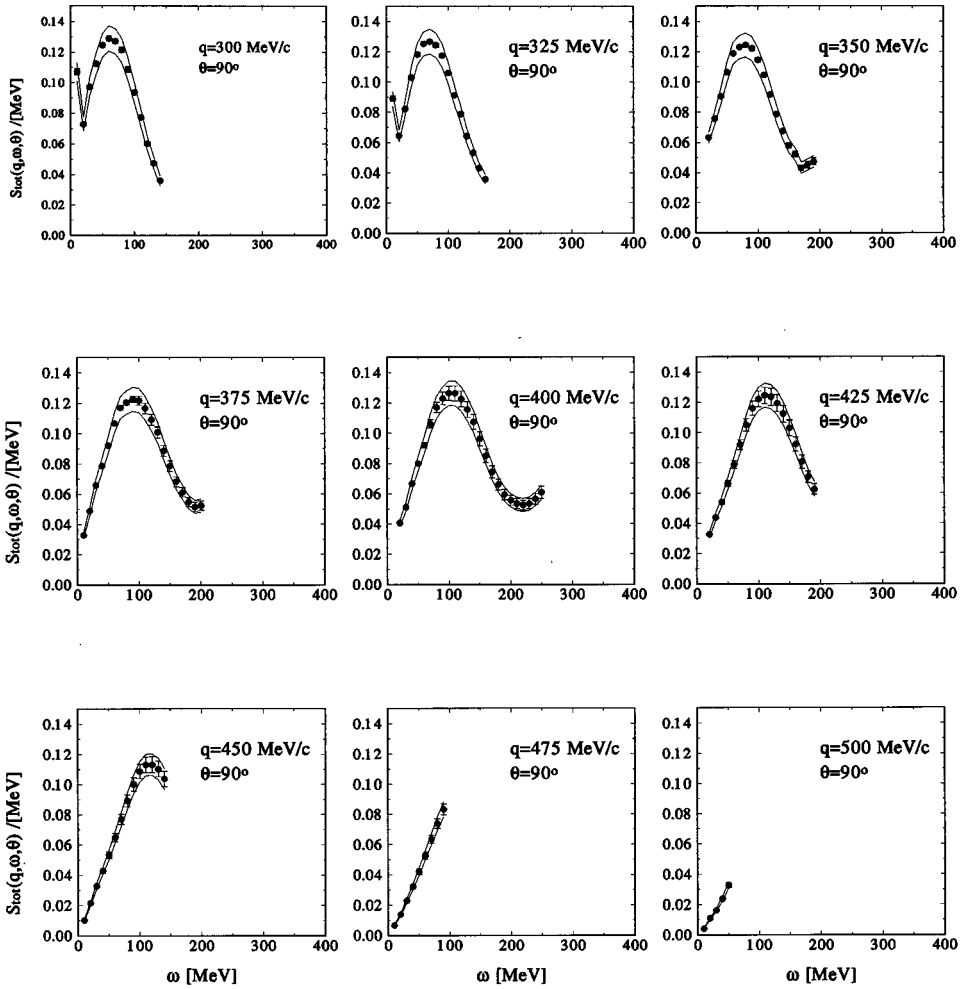

FIG. 10. Same as Fig. 9 for a laboratory scattering angle of 90°. Statistical errors on the individual points are shown as error bars.

entire range of kinematically accessible values of energy loss. In practice this is almost never totally achievable. In some cases because of the cutoff imposed by the elastic radiative tail, some longitudinal strength will exist above the largest usable value of energy loss. In the present experiment no attempt was made to extrapolate the strength to unmeasured values of ω since it was not clear how this should be done.

Even in spectra where the radiative tail was not significant in the quasielastic region, the usable range was restricted by the fact that for energy losses much above the quasielastic peak the accuracy of the extracted longitudinal response functions was very poor. The region well above the quasielastic peak is dominated by Δ-isobar and meson exchange current effects which are overwhelmingly transverse in nature. Therefore, extracting the longitudinal responses in this kinematic region by the Rosenbluth method results in relatively large errors being assigned to the relatively small longitudinal responses. It is not profitable to extend the integration over a kinematic region where the errors are comparable to or larger than the longitudinal responses themselves since this would result in an increased error with little change in the value of the longitudinal strength. Thus, the integration was terminated at an energy loss at which the errors were essentially equal to the response functions. This is a somewhat arbitrary procedure, but the total strengths so determined were found to be insensitive to the cutoff energy for ''reasonable'' choices.

These experimental limitations imply that any longitudinal strength distributed at values of energy loss much above the quasielastic peak will not be included in the reported value of integrated longitudinal strength. This is an inherent limitation in the Rosenbluth method, and integrated longitudinal strengths obtained by this method must always be considered as lower limits.

One could in principle also obtain total integrated strengths for the transverse response. However, these are much more difficult to interpret in a straightforward way. At higher energies in particular, there are significant contributions in the quasielastic region from meson exchange currents and from the tails of the Δ-isobar resonance. These have very small longitudinal components. A fairly unambiguous determination of the longitudinal strengths is therefore obtained by considering only the contribution from quasielastic scattering. The integrated transverse strengths, on the other hand, in general include very significant contributions from other excitation mechanisms. Interpretations of the integrated strengths would require very model-dependent calculations of these mechanisms. The existing theories cannot account for the shape of the transverse responses, especially in the region between the quasielastic peak and the Δ resonance. Therefore, it was felt that a comparison of mea-

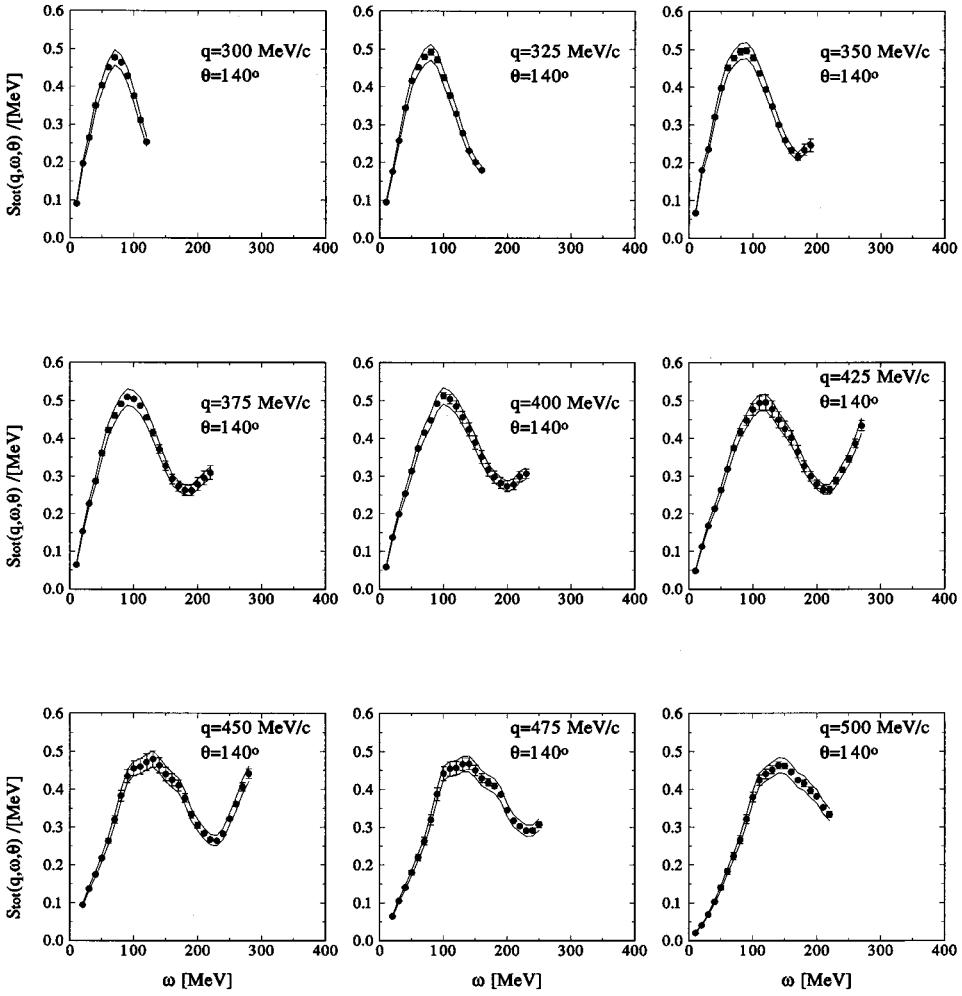

FIG. 11. Same as Fig. 10 for a laboratory scattering angle of 140°.

sured integrated transverse strengths to theoretical ones would not be very useful.

VII. RESULTS AND DISCUSSION

A. Response functions

As described in the previous section, a number of corrections had to be applied to the experimental spectra. An example of a spectrum at three stages in the analysis process is displayed in Fig. 5. This is a spectrum at a bombarding energy of 372 MeV observed at a laboratory scattering angle of 90°. This particular spectrum required all the corrections described in the previous section, and it had the largest correction of any spectrum taken in this experiment. In particular it required significant corrections both for pion contribution and slit scattering. Data points are shown by the symbols, and the spline curves are intended to guide the eye.

The diamonds and the solid line give the spectrum of scattered electrons corrected only for the efficiencies of the detectors. The squares and dotted line show the spectrum after it has been successively corrected for pion contributions, pair-produced electrons, slit scattering, and the elastic radiative tail. The circles and dashed line show the final spectrum after iteratively unfolding the previous spectrum to correct for inelastic radiative effects.

The corrected spectra for the three scattering angles observed in this experiment are shown in Figs. 6–8. A fairly complete set of spectra was obtained at 45.5° and 140°, but accelerator running time constraints allowed only a restricted set of data at 90°. All these spectra exhibit a clear quasielastic peak. The higher-energy spectra, especially at 45.5°, exhibit evidence of the Δ-isobar resonance. However, the kinematic range of this experiment was not sufficient to allow a systematic study of Δ excitation in nuclei. In all spectra the solid lines indicate the estimated instrumental error band. The statistical error bars were smaller than the data symbols.

The experimental cross sections were then interpolated to give response functions at constant three-momentum transfers. These were extracted on a grid of 25 MeV/c steps in q and 10 MeV steps in ω from 300 to 500 MeV/c. The results are shown in Figs. 9–11. The solid lines indicate the estimated instrumental error band and the vertical error bars indicate the statistical error. The range of the data cover essentially the entire quasielastic peak up to a momentum transfer of 475 MeV/c at 45.5° and 140°. However, the 90° data cover the entire quasielastic peak only for momentum transfers up to approximately 400 MeV/c.

The response functions at constant q at the three experimental scattering angles were the basis for Rosenbluth sepa-

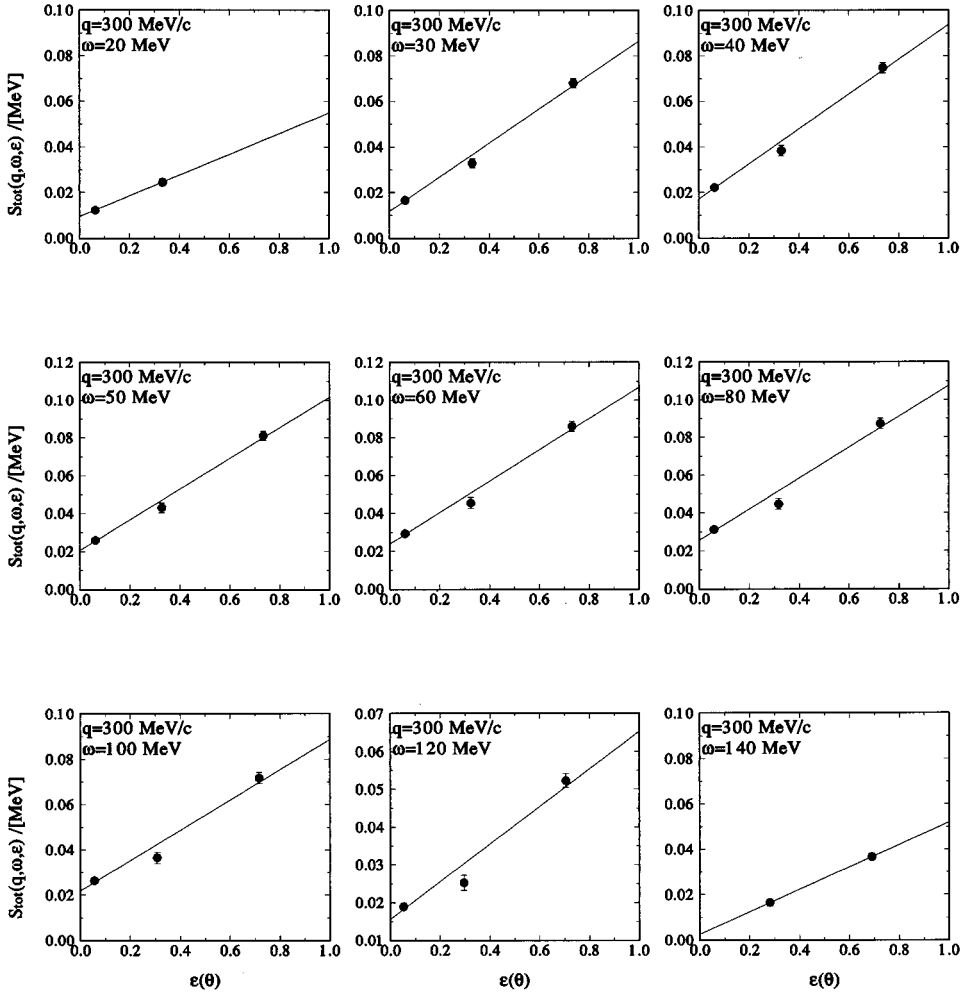

FIG. 12. Rosenbluth plots for a constant three-momentum transfer of 300 MeV/c at several energy losses for ^{40}Ca. The error bars indicate the propagated systematic errors.

rations from 300 to 500 MeV/c in 25 MeV/c steps. Selected Rosenbluth separations plotted according to Eq. (5) are shown in Figs. 12–15 for q = 300, 350, 400, and 450 MeV/c. One feature of these Rosenbluth plots is that for 300 and 350 MeV/c some of the responses at 90° lie significantly below the fitted straight line. As noted in Sec. V the 90° data were taken with a plastic Čerenkov detector that could not discriminate against pions whose momenta corresponded to those of electrons with energy losses above the quasielastic peak. The data taken at this angle required more corrections than those taken at the other two angles and were thus assigned a larger instrumental error. It is also clear from these figures that many of the separations at large q and ω were determined only by the data at 45.5° and 140°.

The longitudinal response functions extracted from these data are shown in Fig. 16. The solid lines are the calculated responses based on the relativistic Fermi gas model [75]. It is immediately clear that the relativistic Fermi gas model does not give an accurate description of the shape or peak position of the longitudinal responses. The peaks of the measured response functions are in general somewhat shifted to higher energy losses than predicted by the relativistic Fermi gas model. Furthermore, the measured distributions appear to be wider in energy loss than predicted by the relativistic Fermi gas model. The dashed lines in Fig. 16 are the calculated responses based on the relativistic Hartree shell model [76]. The overall agreement of these calculations with the experimental data is quite good except for the responses at 300 MeV/c.

The transverse response functions extracted from these data are shown in Fig. 17. At low values of q both the relativistic Fermi gas model and the relativistic Hartree shell model overestimate the magnitude of the response functions. At higher values of q both models do better at reproducing the magnitudes of the response functions. However, it is clear that the relativistic Hartree shell model gives a superior reproduction of the shapes of the response functions at energy losses up to the quasielastic peak. It is evident that there are contributions to the transverse response functions from processes other than quasielastic scattering at energy losses above the quasielastic peak. No process other than quasielastic scattering is included in the theoretical models.

The apparent failures of the relativistic Fermi gas model are not surprising. This model contains no nucleon-nucleon correlation effects other than the Pauli principle for a confined Fermi gas. It can therefore not generate momentum components beyond those required by the simple confinement of the gas. Real nuclei are certainly more complicated

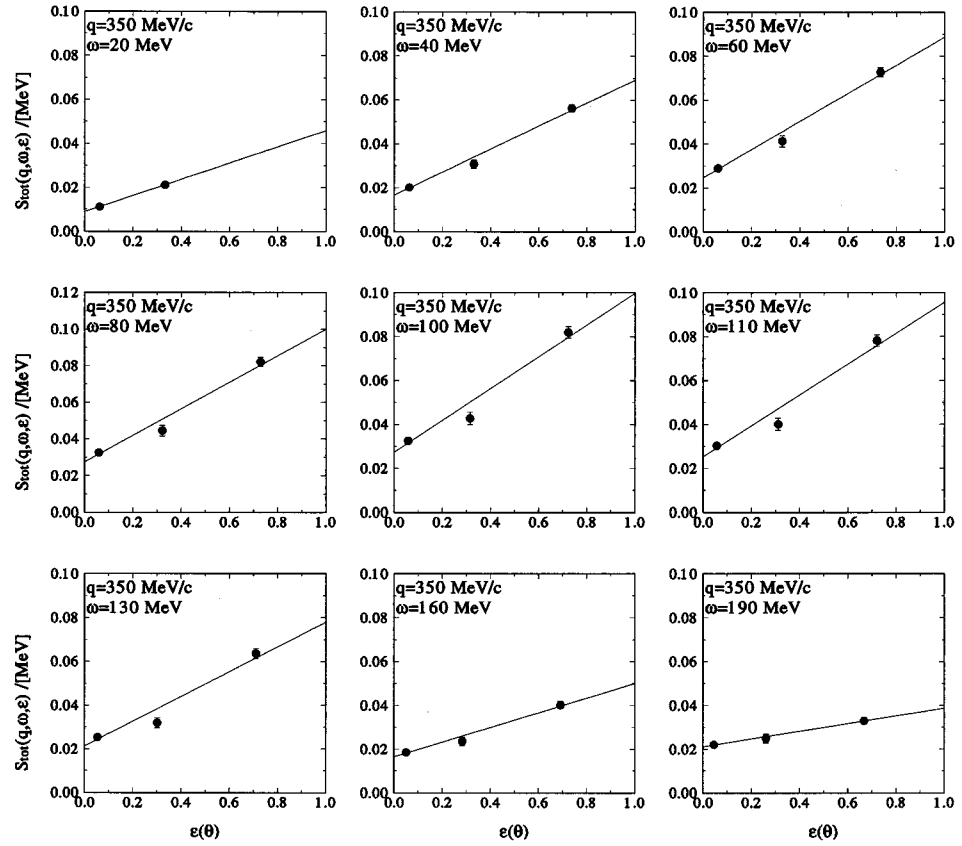

FIG. 13. Rosenbluth plots for a constant three-momentum transfer of 350 MeV/c at several energy losses for ^{40}Ca. The error bars indicate the propagated systematic errors.

than this in their internal correlations. Furthermore, in its truly covariant form, the relativistic Fermi gas has a negative nucleon separation energy. Real nuclei are in fact bound systems and have positive separation energies. It is therefore not surprising that the position of the quasielastic peak is not accurately reproduced.

These deficiencies are partially remedied in the relativistic Hartree shell model calculations. The nuclear wave functions are the result of a self-consistent calculation using realistic nuclear potentials. The calculation is gauge invariant in that both the initial bound state wave functions and the final unbound state wave functions are generated from the same potential. These calculations reproduce the shape and position of the quasielastic peak much better than the relativistic Fermi gas model.

In spite of its shortcomings, the relativistic Fermi gas model does have the possibility of describing with reasonable accuracy the total strength of the quasielastic interaction in the kinematic domain where incoherent scattering is expected to be dominant. To first order, the total strength will be the incoherent sum of the scatterings from all the nucleons. This can be calculated with good accuracy based on measured transverse and longitudinal form factors of the nucleon. Short-range correlations can redistribute the calculated strength in ω, but they do not change the total strength. Therefore, a comparison of the total measured quasielastic strength to that predicted by the relativistic Fermi gas model should be meaningful. As noted above, the longitudinal responses are probably the only ones that are useful for such a comparison since the transverse responses contain strong contributions from processes other than quasielastic scattering.

Preliminary results of such a comparison were made for the present data in Ref. [1] and are reproduced in Fig. 2 above. These data have been completely reanalyzed with some modest improvements in the data reduction codes. The final results are shown in Fig. 18. Also shown are the corresponding results from Meziani *et al.* [48]. This figure clearly shows the discrepancies between the present Bates results and the previous Saclay results. The Bates data indicate a reduction in the longitudinal strength of no more than about 18% at $q = 450$ MeV/c, whereas the Saclay data indicate as much as 40% reduction in the longitudinal strength compared to the prediction of the relativistic Fermi gas model. A reduction of this magnitude is very difficult to understand in the framework of conventional nuclear physics.

The Bates and Saclay groups have cooperated closely in attempting to resolve this discrepancy. The Saclay data for the radiatively corrected cross sections were analyzed using the Bates codes. The results reproduced accurately the Saclay results. It was therefore concluded that the discrepancies were not due to this part of the analysis. Unfortunately, it was not possible to check the radiative correction part of the analysis since the uncorrected Saclay cross sections apparently are no longer available. Since the radiative corrections are a fairly straightforward procedure, it is unlikely that they are the source of the discrepancy. We therefore con-

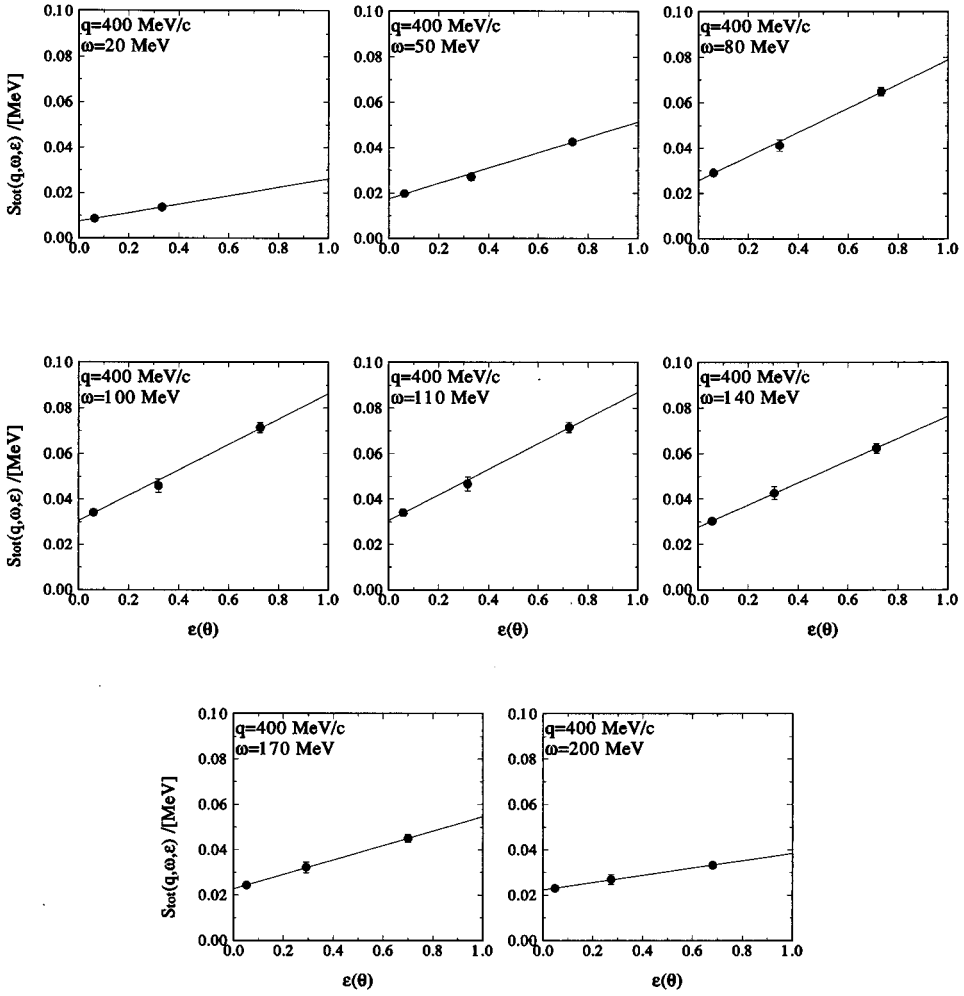

FIG. 14. Rosenbluth plots for a constant three-momentum transfer of 400 MeV/c at several energy losses for ^{40}Ca. The error bars indicate the propagated systematic errors.

clude that it is most likely that the differences lie in the raw data themselves.

Recent theoretical quasielastic scattering calculations by Amaro *et al.* [77] and by Van der Sluys *et al.* [78] have included meson exchange currents. In both of these calculations the calculated longitudinal response functions are in reasonably good agreement with the latest Bates data. The calculations of Ref. [77] are also in reasonable agreement with the present transverse response functions. The calculated transverse response functions of Ref. [78] lie about 25% higher than the present data. None of these theoretical calculations is in agreement with the data of Ref. [49]. These calculations are interesting and informative, but unfortunately they cannot resolve the question of the discrepancies between the two data sets.

A reanalysis of the world data for quasielastic scattering on ^{56}Fe and ^{40}Ca has been carried out by Jourdan [79]. In the case of ^{56}Fe the data set included the measurements of Day *et al.* [80] taken at SLAC at laboratory scattering angles between 15° and 30°. The analysis of the ^{56}Fe data indicated no significant reduction of the longitudinal strength compared to the predictions of the relativistic Fermi gas model. Unfortunately, the measurements of Ref. [80] did not include ^{40}Ca as a target. However, the equivalent ^{40}Ca structure functions were calculated in Ref. [79] by interpolation of data from other nuclei. The resulting longitudinal strengths showed no significant deviations from the strengths expected on the basis of the relativistic Fermi gas model. Because they are the result of interpolation and not of actual data, these comparisons for ^{40}Ca unfortunately do not have the same level of credibility as the ^{56}Fe comparisons.

B. The Coulomb sum rule

The total longitudinal strength in quasielastic electron scattering has been traditionally compared to the Coulomb sum rule $R_i(q)$. Including the relativistic corrections of de Forest [83], this can be written as

$$R_i(q)=\frac{1}{Z}\int_{\omega^+}^{\infty}\frac{R_L(q,\omega)}{\widetilde{G}_E{}^2(Q^2)}d\omega, \tag{13}$$

with the effective electric form factor given by

$$\widetilde{G}_E{}^2(Q^2)=\left[G_{Ep}{}^2(Q^2)+\frac{N}{Z}G_{En}{}^2(Q^2)\right]\frac{(1+\tau)}{(1+2\tau)},$$

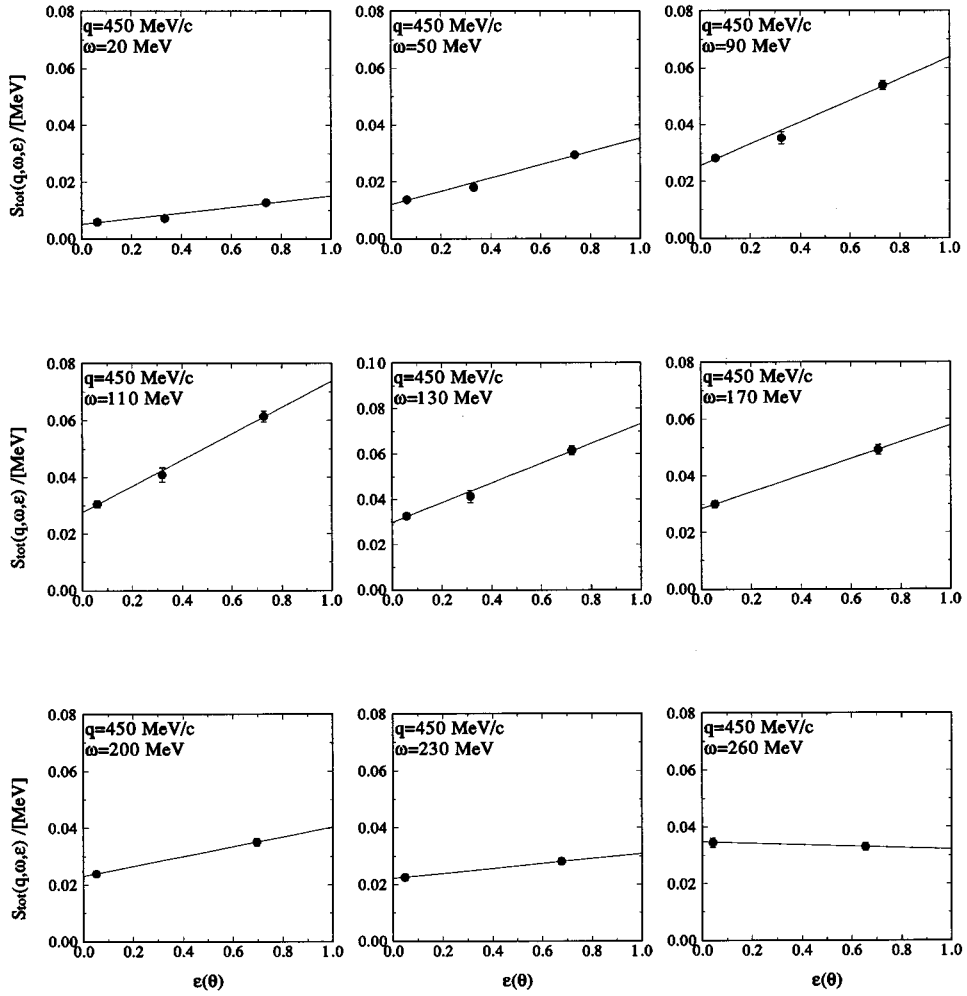

FIG. 15. Rosenbluth plots for a constant three-momentum transfer of 450 MeV/c at several energy losses for ^{40}Ca. The error bars indicate the propagated systematic errors.

where N and Z are the neutron and proton numbers of the target, respectively, and G_{Ep} and G_{En} are the Sachs electric form factors for the proton and neutron, respectively. The quantity τ is given by $\tau = Q^2/4M_N{}^2$, where M_N is the nucleon mass. The lower limit of integration ω^+ is chosen to include all the inelastic strength but to exclude the elastic peak. All other symbols have been previously defined. A value of unity for $R_i(q)$ indicates fulfillment of the Coulomb sum rule.

The Coulomb sum rule as expressed in Eq. (13) has several shortcomings. It is impossible to measure the response functions for $\omega > q$ (the timelike region) in a single-arm scattering experiment. It is difficult to estimate how much strength is missed in this timelike region. Equation (13) also does not take into account Pauli blocking effects and is not expected to be valid for q less than twice the Fermi momentum (about 480 MeV/c for ^{40}Ca). Finally, it is not clear that the relativistic corrections in Eq. (13) are truly valid for large values of q.

For these reasons, we do not feel that the Coulomb sum rule is a very useful way of characterizing the data. We prefer to compare the data to the predictions of a particular model, such as the relativistic Fermi gas model or the relativistic Hartree shell model. However, since the Coulomb sum rule has become the traditional way of characterizing quasielastic scattering data, we present the results of applying Eq. (13) to the present data in Fig. 19. Also presented in Fig. 19 for comparison is the corresponding Coulomb sum rule for the relativistic Fermi gas model.

The results shown in Fig. 19 are qualitatively the same as those shown in Fig. 18. At the lower values of q both the data and the relativistic Fermi gas model fail to exhaust the Coulomb sum rule, although they agree quite well with one another. At larger values of q, the relativistic Fermi gas model does exhaust the Coulomb sum rule, whereas the data fail to exhaust this sum rule by about 15%. A similar effect is seen in Fig. 18, and in both cases this may indicate the presence of longitudinal strength beyond the experimental cutoff values of ω.

C. Scaling

Many classes of natural phenomena exhibit the property known as scaling. Scaling is manifested when the apparently independent variables upon which a phenomenon depends are functionally related in an underlying manner such that the phenomenon can actually be described by fewer (ideally one) independent variables. In the case of quasielastic scat-

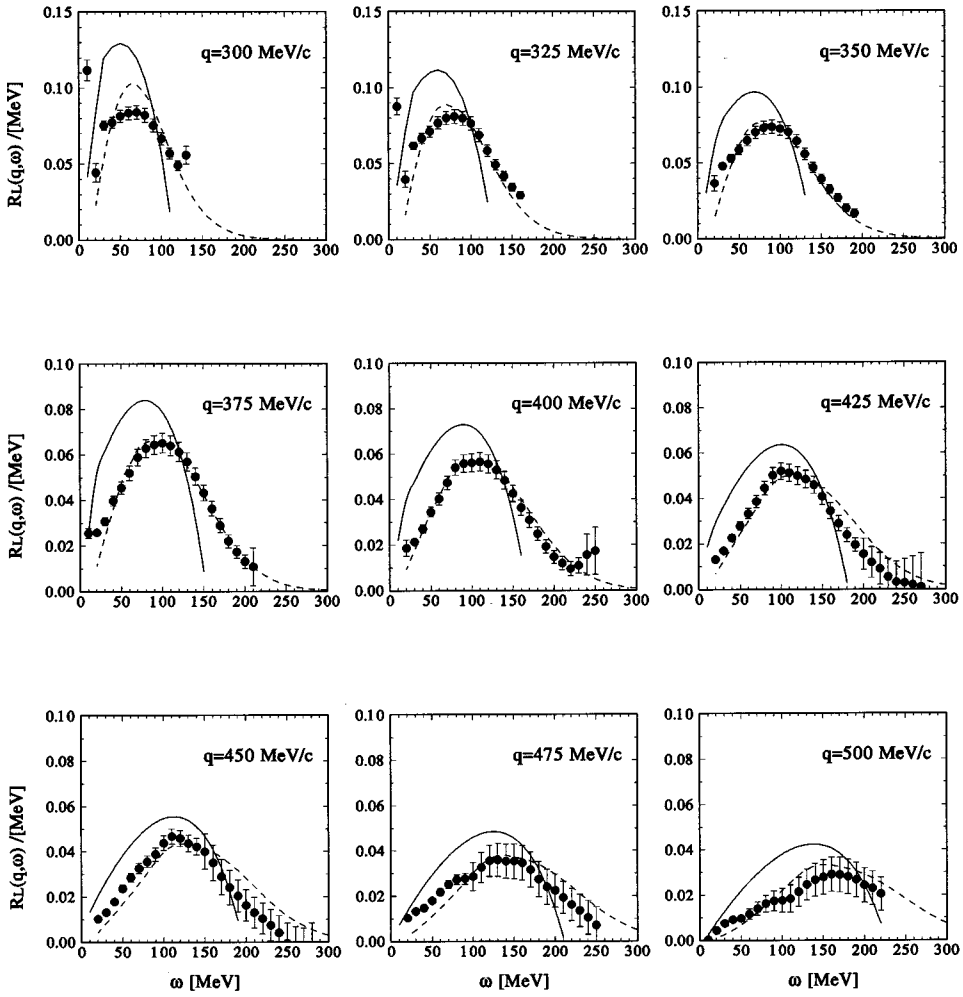

FIG. 16. Longitudinal response functions extracted from the present data for ^{40}Ca over the three-momentum transfer range 300–500 MeV/c. The error bars indicate the propagated systematic errors. The solid curves were calculated from the relativistic Fermi gas model [75], and the dashed curves were calculated from the relativistic Hartree shell model [76]

tering the response functions are apparently dependent upon two independent variables q and ω. However, a number of authors have explored the possibility that there is an underlying relationship between these variables in quasielastic scattering, and a number of scaling variables have been proposed. For example, a subset of the present data was used as a test of the y-scaling function [81].

A scaling variable ψ was defined by Alberico *et al.* [75] in such a manner that if the relativistic Fermi gas were an exact description of nuclear structure, then all quasielastic response functions would scale exactly according to this variable. In this section the formalism will be that of Ref. [75], and therefore the definitions of the mathematical symbols will not be repeated here.

It is shown in Ref. [75] that in the framework of the relativistic Fermi gas model one can define a scaling variable ψ that maps the separated response functions into parabolas as

$$\psi=[2\,\theta(\lambda-\lambda_0)-1]\sqrt{\frac{1}{\xi_F}(\gamma_--1)}.$$

This then leads to a scaling function $S(\psi)$ of the form

$$S(\psi)=\frac{3}{4}(1-\psi^2)\,\theta(1-\psi^2), \tag{14}$$

where $\theta(x-a)$ is the unit step function at a. The scaling function defined in this manner is normalized such that

$$\int_{-1}^{+1} S(\psi)\,d\psi=1.$$

The scaling function is related to the longitudinal and transverse response functions by

$$R_L=\sum_i \frac{N_i\xi_F}{M_{Ni}\kappa\,\eta_F^3}[G_{Ei}^2(\tau)+W_{2i}(\tau)\Delta]S(\psi), \tag{15}$$

$$R_T=\sum_i \frac{N_i\xi_F}{M_{Ni}\kappa\,\eta_F^3}\left[\tau G_{Mi}^2(\tau)+\frac{1}{2}W_{2i}(\tau)\Delta\right]S(\psi), \tag{16}$$

where $G_{Ei}(\tau)$ and $G_{Mi}(\tau)$ are the Sachs electric and magnetic form factors, respectively, for the ith nuclear species.

An extension of the relativistic Fermi gas model was made by Cenni *et al.* [82] to include effects of nuclear bind-

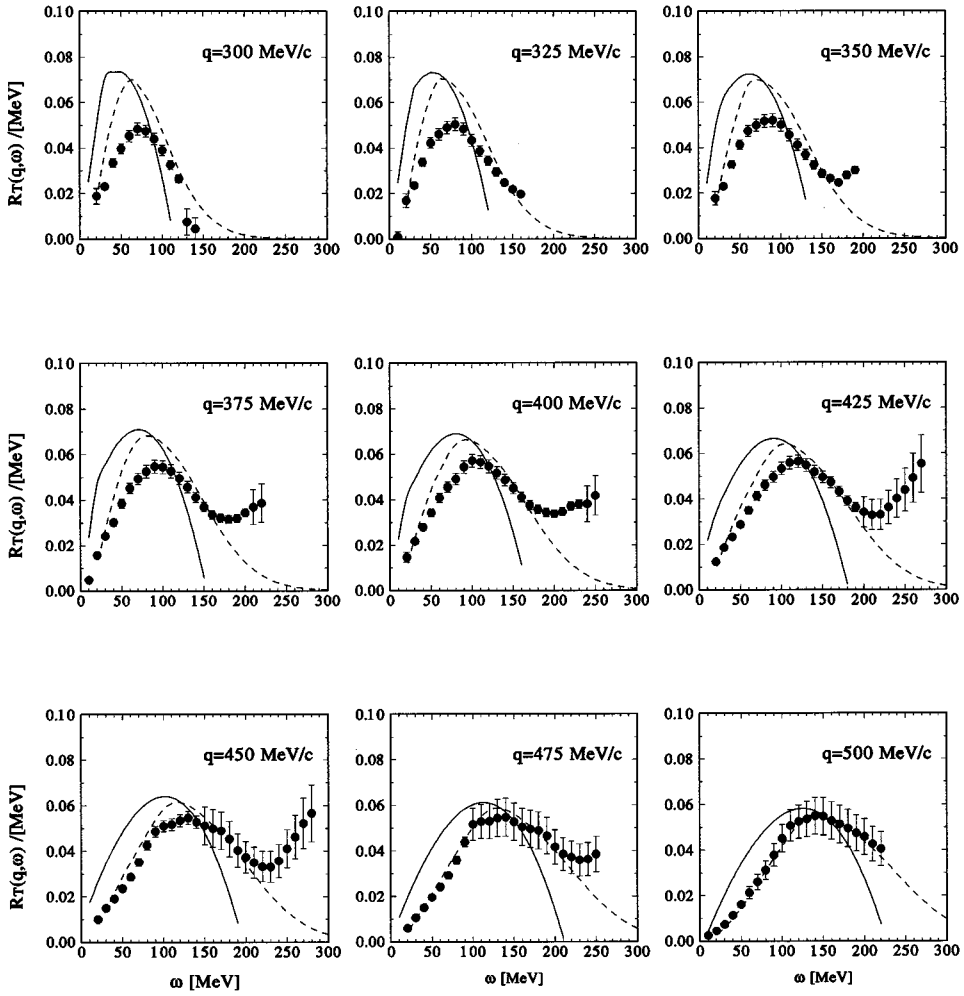

FIG. 17. Same as for Fig. 16 but showing the transverse response functions.

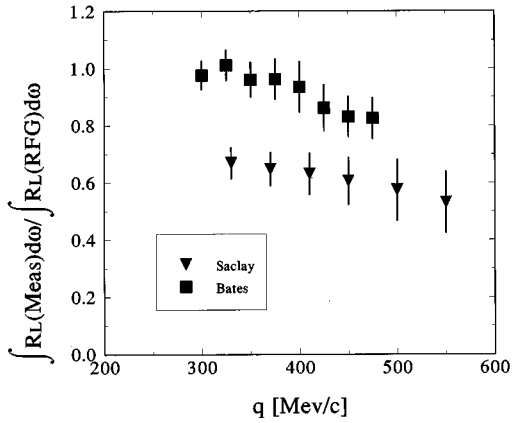

FIG. 18. Ratio of experimental integrated longitudinal response functions to the total longitudinal strength calculated from the relativistic Fermi gas model for ^{40}Ca. The solid squares are the present data and the solid triangles are the results of Meziani *et al.* [49]. The present results are given in tabular form in Table II.

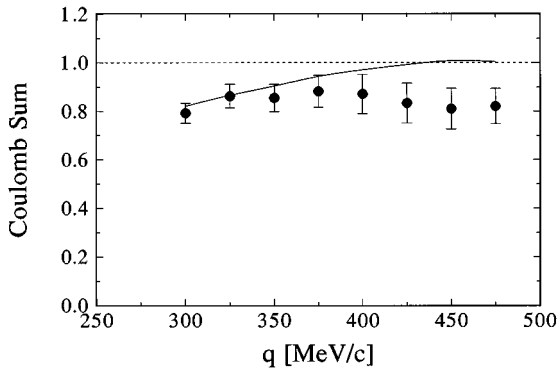

FIG. 19. The Coulomb sum rule for ^{40}Ca. The solid circles are calculated from the data of the present experiment. The solid line is the sum rule calculated from relativistic Fermi gas calculations. The dashed curve is the theoretical sum rule for the independent particle model with relativistic corrections.

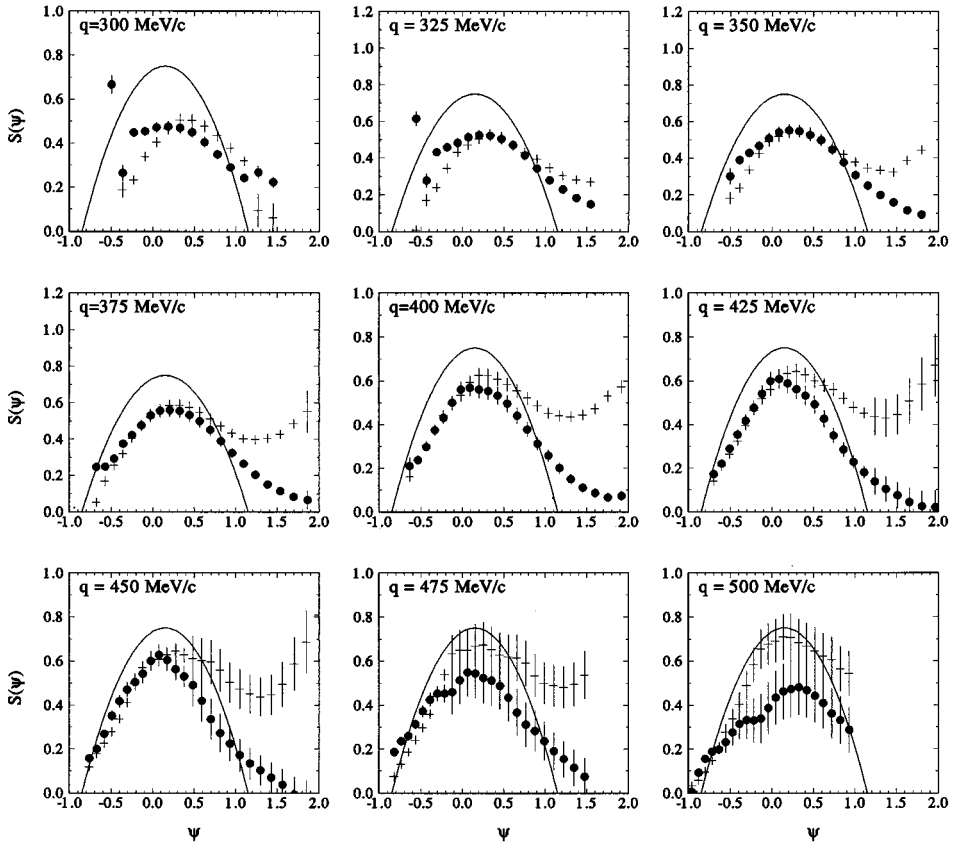

FIG. 20. ψ'-scaled response functions for ^{40}Ca. The experimental response functions were scaled according to Eqs. (15) and (16) as modified by Eq. (17). The scaled longitudinal response functions are shown as circles, and the scaled transverse response functions are shown as crosses. The solid curves are the predictions of the relativistic Fermi gas model.

ing at the cost of a slight loss of relativistic covariance. Within the framework of this model, one can define a new scaling variable ψ'. This scaling variable has the same form as ψ if one makes the following substitutions:

$$\omega' = \omega - (E_S + T_F), \tag{17}$$

where

E_S = nucleon separation energy,

$$T_F = M_N\left(-1+\sqrt{1+\left(\frac{p}{M_N}\right)^2}\right).$$

It turns out that $S(\psi)$ and $S(\psi')$ have almost exactly the same shape and magnitude, but $S(\psi')$ gives a much better fit to the position of the quasielastic peak.

The experimentally determined scaling functions can be determined from Eqs. (15) and (16) (with the substitution $\psi \rightarrow \psi'$) from the experimentally determined values of R_L

TABLE II. Integrated longitudinal strength as a function of three-momentum transfer q. Column 2 indicates the maximum energy loss to which the longitudinal strength was integrated. Columns 3 and 4 give the integrated experimental longitudinal strength and its systematic uncertainty, respectively. Column 5 presents the total longitudinal strength calculated from the relativistic Fermi gas model. Columns 6 and 7 show the ratio of the experimental to the theoretical longitudinal strength and its uncertainty, respectively. These ratios are given graphically in Fig. 18.

q[MeV/c]	$\omega_{\max}$[MeV]	$\Sigma R_L^{(\exp)}$	$\delta(\Sigma R_L^{(\exp)})$	$\Sigma R_L^{(\mathrm{RFG})}$	Ratio	δ(Ratio)
300.0	140.0	9.92	0.52	10.16	0.977	0.052
325.0	160.0	10.04	0.55	9.92	1.012	0.056
350.0	190.0	9.18	0.60	9.55	0.961	0.062
375.0	220.0	8.83	0.66	9.17	0.963	0.072
400.0	250.0	8.08	0.78	8.64	0.935	0.090
425.0	260.0	6.95	0.67	8.07	0.862	0.083
450	240.0	6.21	0.55	7.47	0.831	0.073
475.0	230.0	5.64	0.50	6.84	0.826	0.074

and R_T. If $S(\psi')$ were truly a universal scaling function, its form as determined from Eqs. (15) and (16) should be the same for both R_L and R_T. If nuclear dynamics were truly described by the relativistic Fermi gas model, then the experimentally determined scaling function would be described by Eq. (14).

The scaling functions $S(\psi')$ have been extracted from the experimental data using Eqs. (15) and (16). The results are shown in Fig. 20 in increments of q of 25 MeV/c over the range from 300 to 500 MeV/c. It is clear from this figure that in the range 375 MeV $\leqslant q \leqslant$ 450 MeV/c for values of ψ' smaller than those corresponding to the quasielastic peak, the values of $S(\psi')$ extracted from the transverse and longitudinal responses agree to within the experimental errors. The agreement is lost for values of ψ' larger than those corresponding to the quasielastic peak. This is not surprising since one expects in this kinematic range to observe significant contributions to the transverse response from processes other than quasielastic scattering.

The agreement for values of q less than 375 MeV/c is not as good, and it becomes worse as q decreases. This is also not surprising since at these lower momentum transfers the wavelength of the virtual photon is not short enough to ensure incoherent scattering from individual nucleons. An appreciable portion of the strength may be diverted to excitation of coherent degrees of freedom in the nucleus corresponding to low-lying states.

For $q \geqslant$ 475 MeV/c the $S(\psi')$ values extracted from the transverse responses lie significantly above those extracted from the longitudinal responses. It is unclear whether this reflects the onset of new physics or simply reflects an increasing dominance in the transverse response of nonquasielastic processes.

The ψ' scaling variable is based on the relativistic Fermi gas model, but the data do not scale well to this model. However, the data do seem to indicate that, in the kinematic region where quasielastic scattering is expected to dominate, both the longitudinal and transverse responses scale to the same function. Therefore, there may be deeper physical significance to the scaling variable ψ' than would be expected from its roots in the relativistic Fermi gas model.

VIII. CONCLUSIONS

The results reported here of the total longitudinal strength in quasielastic electron scattering from ^{40}Ca are in sharp contrast to the previously reported Saclay results. The Saclay results show a reduction of as much as 40% in the integrated longitudinal strength compared to the predictions of the relativistic Fermi gas model. The present data show a much smaller reduction in the integrated longitudinal strength as indicated by Table II. The general trend of the integrated strength seems to be a systematic decrease with increasing q. This may be due to the fact that at larger momentum transfer some strength is missed due to the necessity of cutting off the integrals of the response functions at finite ω.

The implications of the above observations for conventional nuclear physics are profound depending on which (if either) result is correct. The bibliography contains many theoretical attempts to explain the large reduction reported by the Saclay group. In general, the results may be summarized by stating that it has been found to be almost impossible to fit both the longitudinal and transverse response functions reported by Saclay by nuclear models using physically reasonable parameters. On the other hand, the modest reductions reported here are easily accommodated by many conventional nuclear model calculations.

We consider it very important that the question of the longitudinal strength in quasielastic electron scattering be cleanly resolved. This would require precision measurements over a kinematic range that would allow Rosenbluth separations from 300 MeV/$c \leqslant q \leqslant$ 700 MeV/c for several nuclei in the range $12 \leqslant A \leqslant 238$ at four or more laboratory scattering angles. Such a set of measurements, if carefully performed, should lead to reliable separation of the transverse and longitudinal responses as a function of energy loss, the behavior of their integrated strengths as a function of momentum transfer, and the dependence of these strengths on nuclear mass.

[1] T. C. Yates *et al.*, Phys. Lett. B **312**, 382 (1993).
[2] H. F. Ehrenberg and R. Hofstadter, Phys. Rev. **110**, 544 (1958).
[3] J. E. Leiss and R. E. Taylor, in *Contributions to the Karlsruhe Photonuclear Conference, 1960* (E. P. I. der Universität Heidelberg, Heidelberg, 1960).
[4] P. Bounin and G. R. Bishop, J. Phys. Radium **22**, 555 (1961).
[5] G. R. Bishop, D. B. Isabelle, and C. Betourne, Nucl. Phys. **54**, 97 (1964).
[6] H. Nguyen-Ngoc and J. P. Perez-Y-Jorba, Phys. Rev. Lett. **136**, B1036 (1964).
[7] J. Berthot and D. B. Isabelle, Lett. Nuovo Cimento **5**, 155 (1972).
[8] J. Berthot and D. B. Isabelle, Rev. Phys. Appl. **7**, 413 (1972).
[9] S. Klawansky, H. W. Kendall, A. Kerman, and D. B. Isabelle, Phys. Rev. C **7**, 795 (1973).
[10] W. L. Faissler, F. M. Pipkin, and K. C. Stanfield, Phys. Rev. Lett. **19**, 1202 (1967).
[11] K. C. Stanfield, C. R. Canizares, W. L. Faissler, and F. M. Pipkin, Phys. Rev. C **3**, 1448 (1971).
[12] S. V. Dementii *et al.*, Sov. J. Nucl. Phys. **9**, 142 (1969).
[13] Y. I. Titov *et al.*, Sov. J. Nucl. Phys. **9**, 772 (1969).
[14] Y. I. Titov *et al.*, Sov. J. Nucl. Phys. **11**, 145 (1970).
[15] Y. I. Titov *et al.*, Sov. J. Nucl. Phys. **13**, 660 (1971).
[16] Y. I. Titov and E. V. Stepula, Sov. J. Nucl. Phys. **15**, 361 (1972).
[17] F. H. Heimlich *et al.*, Nucl. Phys. **A231**, 509 (1974).
[18] W. Czyz and K. Gottfried, Ann. Phys. (N.Y.) **47**, 47 (1963).
[19] W. Czyz, Phys. Rev. **131**, 2141 (1963).
[20] A. G. Sitenko and I. V. Simenog, Nucl. Phys. **80**, 643 (1966).
[21] G. R. Henry, Phys. Rev. **151**, 875 (1966).
[22] G. R. Henry, Phys. Rev. **157**, 871 (1967).
[23] T. de Forest, Ann. Phys. (N.Y.) **45**, 365 (1967).
[24] A. Malecki and P. Picchi, Nuovo Cimento A **58**, 145 (1968).
[25] T. de Forest, Jr., Nucl. Phys. **A132**, 305 (1969).

[26] E. J. Moniz, Phys. Rev. **184**, 1154 (1969).
[27] D. H. Freiberg, Phys. Rev. C **1**, 1735 (1970).
[28] T. W. Donnelly, Nucl. Phys. **A150**, 393 (1970).
[29] G. B. West, Phys. Rep. **18**, 263 (1975).
[30] U. Glawe *et al.*, Phys. Lett. **89B**, 44 (1979).
[31] E. J. Moniz *et al.*, Phys. Rev. Lett. **26**, 445 (1971).
[32] R. R. Whitney *et al.*, Phys. Rev. C **9**, 2230 (1974).
[33] P. D. Zimmerman, Ph.D. thesis, Stanford University, 1969.
[34] P. D. Zimmerman and M. R. Yearian, Z. Phys. A **278**, 291 (1976).
[35] Y. Kawazoe, G. Takeda, and H. Matsuzaki, Prog. Theor. Phys. **54**, 1394 (1975).
[36] A. Dellafiore, Nucl. Phys. **A282**, 493 (1977).
[37] F. A. Brieva and A. Dellafiore, Nucl. Phys. **A292**, 445 (1977).
[38] G. Do Dang, Phys. Lett. **69B**, 425 (1977).
[39] J. W. Van Orden, Ph.D. thesis, Stanford University, 1978.
[40] T. W. Donnelly, J. W. Van Orden, T. de Forest, Jr., and W. C. Hermans, Phys. Lett. **76B**, 393 (1978).
[41] R. Rosenfelder, Phys. Lett. **79B**, 15 (1978).
[42] J. W. Van Orden, W. Truex, and M. K. Banerjee, Phys. Rev. C **21**, 2628 (1980).
[43] Y. Horikawa, F. Lenz, and N. C. Mukhopadhyay, Phys. Rev. C **22**, 1680 (1980).
[44] R. Altemus *et al.*, Phys. Rev. Lett. **44**, 965 (1980).
[45] M. Deady *et al.*, Phys. Rev. C **28**, 631 (1983).
[46] M. Deady *et al.*, Phys. Rev. C **33**, 1897 (1986).
[47] P. Barreau *et al.*, Nucl. Phys. **A402**, 515 (1983).
[48] Z. E. Meziani *et al.*, Phys. Rev. Lett. **52**, 2130 (1984).
[49] Z. E. Meziani *et al.*, Phys. Rev. Lett. **54**, 1233 (1985).
[50] J. V. Noble, Phys. Rev. Lett. **46**, 412 (1981).
[51] L. S. Celenza, W. S. Pong, M. M. Rahman, and C. M. Shakin, Phys. Rev. C **26**, 320 (1982).
[52] J. V. Noble, Phys. Rev. C **27**, 423 (1983).
[53] G. Do Dang and P. Van Thieu, Phys. Rev. C **28**, 1845 (1983).
[54] L. S. Celenza, W. S. Pong, and C. M. Shakin, Phys. Rev. C **27**, 2792 (1983).
[55] J. M. Finn, R. W. Lourie, and B. H. Cottman, Phys. Rev. C **29**, 2230 (1984).
[56] G. Do Dang and N. Van Giai, Phys. Rev. C **30**, 731 (1984).
[57] L. S. Celenza, A. Rosenthal, and C. M. Shakin, Phys. Rev. Lett. **53**, 892 (1984).
[58] L. S. Celenza, A. Harindranath, and C. M. Shakin, Phys. Rev. C **32**, 248 (1985).
[59] L. S. Celenza, A. Harindranath, and C. M. Shakin, Phys. Rev. C **32**, 650 (1985).
[60] L. S. Celenza, A. Harindranath, and C. M. Shakin, Phys. Rev. C **33**, 1012 (1986).
[61] G. Do Dang, M. L'Huillier, N. Van Giai, and J. W. Van Orden, Phys. Rev. C **35**, 1637 (1987).
[62] W. Leidmann, G. Orlandini, and M. Traini, Phys. Rev. C **44**, 1705 (1991).
[63] P. D. Zimmerman, Phys. Rev. C **26**, 265 (1982).
[64] C. C. Blatchley *et al.*, Phys. Rev. C **34**, 1243 (1986).
[65] A. Zghiche *et al.*, Nucl. Phys. **A572**, 513 (1994).
[66] W. Bertozzi, J. Haimson, C. P. Sargent, and W. Turchinetz, IEEE Trans. Nucl. Sci. **NS-14**, 191 (1967).
[67] W. Bertozzi *et al.*, Nucl. Instrum. Methods **162**, 211 (1979).
[68] W. Bertozzi *et al.*, Nucl. Instrum. Methods **141**, 457 (1977).
[69] B. Rossi and K. Greisen, Rev. Mod. Phys. **13**, 240 (1941).
[70] L. Landau, J. Phys. VII, **201** (1944).
[71] L. W. Mo and Y. S. Tsai, Rev. Mod. Phys. **41**, 205 (1969).
[72] Y. S. Tsai, Stanford Linear Accelerator Technical Report No. SLAC-PUB-848, 1971 (unpublished).
[73] L. C. Maximon and S. E. Williamson, National Bureau of Standards Internal Report No. NBS-IR-83-2788, 1983 (unpublished).
[74] L. E. Wright (private communication).
[75] W. M. Alberico *et al.*, Phys. Rev. C **38**, 1801 (1988).
[76] Y. Jin, D. S. Onley, and L. E. Wright, Phys. Rev. C **45**, 1333 (1992).
[77] J. E. Amaro, G. Có, and A. M. Lallena, Nucl. Phys. **A578**, 365 (1994).
[78] V. V. der Sluys, J. Ryckenbusch, and M. Waroquier, Phys. Rev. C **51**, 2664 (1995).
[79] J. Jourdan, Nucl. Phys. **A603**, 117 (1996).
[80] D. Day *et al.*, Phys. Rev. C **48**, 1849 (1993).
[81] P. D. Zimmerman, C. F. Williamson, and Y. Kawazoe, Phys. Rev. C **19**, 279 (1979).
[82] R. Cenni, T. W. Donnelly, and A. Molinari, Phys. Rev. C **56**, 276 (1997).
[83] T. de Forest, Nucl. Phys. **A414**, 347 (1984).